A novel non-genetic murine model of hyperglycemia and hyperlipidemia-associated aggravated atherosclerosis

Susanne Gaul[1†], PhD; Khurrum Shahzad[2†*], PhD; Rebekka Medert[3,5†], PhD; Ihsan Gadi[2], Christina Mäder[1], Dagmar Schumacher, PhD[3, 5]; Angela Wirth[3], PhD; Saira Ambreen[2], Sameen Fatima[2], Jes-Niels Boeckel[1], PhD, Hamzah Khawaja[2], Jan Haas[4,5], PhD; Maik Brune[6], MD; Peter P Nawroth[6], Prof., MD; Berend Isermann[2#], Prof., MD; Ulrich Laufs[1#], Prof., MD; Marc Freichel[3, 5#*], Prof., MD

[1] Klinik und Poliklinik für Kardiologie, Universitätsklinikum Leipzig, Leipzig, Germany

[2] Laboratory Medicine, Clinical Chemistry and Molecular Diagnostic, University Hospital Leipzig, Leipzig, Germany

[3] Institute of Pharmacology, Heidelberg University, Heidelberg, Germany

[4] Department of Internal Medicine III, Heidelberg University, Heidelberg, Germany

[5] DZHK (German Centre for Cardiovascular Research), partner site Heidelberg/Mannheim, Germany

[6] Internal Medicine I and Clinical Chemistry, German Diabetes Center (DZD), Heidelberg University, Heidelberg, Germany

*** Correspondence:**
Khurrum Shahzad
Institute of Laboratory Medicine, Clinical Chemistry and Molecular Diagnostic, University Hospital, Leipzig, Liebigstr.27, Leipzig 04103, Germany,
Email: khurrum.shahzad@medizin.uni-leipzig.de

Marc Freichel
Institute of Pharmacology, Heidelberg University, Im Neuenheimer Feld 366, 69120 Heidelberg, Germany;
Email: Marc.freichel@pharma.uni-heidelberg.de

† These authors have contributed equally to this work and share first authorship

# These authors have contributed equally to this work and share last authorship

Keywords: animal model of disease, atherosclerosis, diabetes, hyperglycemia, hyperlipidemia, PCSK9, Streptozotocin

Abstract

Objective: Atherosclerosis, the main pathology underlying cardiovascular diseases is accelerated in diabetic patients. Genetic mouse models require breeding efforts which are time-consuming and costly. Our aim was to establish a new nongenetic model of inducible metabolic risk factors that mimics hyperlipidemia, hyperglycemia, or both and allows the detection of phenotypic differences dependent on the metabolic stressor(s).

Methods and Results: Wild-type mice were injected with gain-of-function $PCSK9^{D377Y}$ (proprotein convertase subtilisin/kexin type 9) mutant adeno-associated viral particles (AAV) and streptozotocin and fed either a high-fat diet (HFD) for 12 or 20 weeks or a high-cholesterol/high-fat diet (Paigen diet, PD) for 8 weeks. To evaluate atherosclerosis, two different vascular sites (aortic sinus and the truncus of the brachiocephalic artery) were examined in the mice. Combined hyperlipidemic and hyperglycemic (HGHCi) mice fed a HFD or PD displayed characteristic features of aggravated atherosclerosis when compared to hyperlipidemia (HCi HFD or PD) mice alone. Atherosclerotic plaques of HGHCi HFD animals were larger, showed a less stable phenotype (measured by the increased necrotic core area, reduced fibrous cap thickness, and less α-SMA-positive area) and had more inflammation (increased plasma IL-1β level, aortic pro-inflammatory gene expression, and MOMA-2-positive cells in the BCA) after 20 weeks of HFD. Differences between the HGHCi and HCi HFD models were confirmed using RNA-seq analysis of aortic tissue, revealing that significantly more genes were dysregulated in mice with combined hyperlipidemia and hyperglycemia than in the hyperlipidemia-only group. The HGHCi-associated genes were related to pathways regulating inflammation (increased *Cd68*, *iNos*, and *Tnfa* expression) and extracellular matrix degradation (*Adamts4* and *Mmp14*). When comparing HFD with PD, the PD aggravated atherosclerosis to a greater extent in mice and showed plaque formation after 8 weeks. Hyperlipidemic and hyperglycemic mice fed a PD (HGHCi PD) showed less collagen (Sirius red) and increased inflammation (CD68-positive cells) within aortic plaques than hyperlipidemic mice (HCi PD). HGHCi-PD mice represent a directly inducible hyperglycemic atherosclerosis model compared with HFD-fed mice, in which atherosclerosis is severe by 8 weeks.

Conclusion: We established a nongenetically inducible mouse model allowing comparative analyses of atherosclerosis in HCi and HGHCi conditions and its modification by diet, allowing analyses of multiple metabolic hits in mice.

Introduction

Atherosclerotic cardiovascular diseases, including coronary artery disease (CAD) and its complications, are a leading cause of mortality and morbidity globally (1). The risk of CAD is markedly increased in patients with both type 1 and type 2 diabetes mellitus (DM), with CAD events occurring earlier in patients with diabetes mellitus (2). Approximately 10% of total vascular deaths have been attributed to diabetes mellitus and its complications (2). Despite recent studies showing cardioprotective effects of new antidiabetic agents (3), there is a high need to understand how diabetes-associated alterations, particularly the evoked chronic hyperglycemia and metabolic alterations, aggravate atherosclerosis in CAD patients as a basis for the development of more effective treatments for these high-risk patients.

Currently used mouse models of hyperglycemia-associated atherosclerosis require a combination of streptozotocin (STZ) and crossbreeding with either apolipoprotein E ($ApoE^{-/-}$) or low-density lipoprotein receptor ($LDLR^{-/-}$) genetic KO mice, or alternatively, a double crossbreeding of $ApoE^{-/-}$ or $LDLR^{-/-}$ with insulin receptor ($Ins2^{+}$, Akita) mutant mice (4). Some murine models, such as STZ-injected human apoB-expressing transgenic mice (5) or nonobese diabetic (NOD) mice (6), are resistant to the development of atherosclerosis. In addition, crossing mouse lines is time-consuming and costly. In particular, if mouse models harboring other genetic manipulations are to be used, backcrossing becomes a major issue. Thus, there is a high demand to generate an inducible mouse model of multiple metabolic hits, e.g., hyperlipidemia and hyperglycemia, which can be used alone or in combination with other genetic modifications. Bjorklund et al. developed a nongenetic mouse model of atherosclerosis induced by a single injection of recombinant adeno-associated virus (rAAV) encoding a hyperactive proprotein convertase subtilisin/kexin type 9 $(PCSK9)^{D377Y}$ mutant followed by high-fat diet (HFD) feeding that has been used in nondiabetic settings (7, 8) as well as in mature diabetic Akita mice, where they showed diabetic-associated accelerated atherosclerosis (7). Here, we combined injections of rAAV8-$PCSK9^{D377Y}$ and STZ with HFD feeding to generate a rapid and versatile method to induce hyperglycemia-induced aggravation of atherosclerosis in mice.

Materials and Methods

All information regarding the materials and reagents is listed in the **Supplementary Major Resources Table**.

Reagents

The following antibodies were used in the current study: rabbit anti-LDLR (R&D Systems, United States); mouse anti-β-actin (Abcepta Inc. United States); goat anti-rabbit IgG HRP (Cell Signaling Technology, Germany); rat anti-MOMA-2, rabbit anti-CD68 and rabbit anti-alpha smooth muscle actin (α-SMA) (Abcam, Germany); and rabbit anti-GAPDH (Sigma–Aldrich, Germany). The following secondary antibodies for immunofluorescence were used: Texas red rabbit anti-mouse

101 IgG (Vector Laboratories, United States) and goat anti-rat IgG (H+L) cross-adsorbed secondary
102 antibody, Alexa Fluor 568 (Thermo Fisher, United States). Other reagents were as follows: BCA
103 reagent (Perbio Science, Germany); vectashield mounting medium with DAPI (Vector
104 Laboratories, United States); nitrocellulose membrane (Bio–Rad, USA) and immobilon^{TM} western
105 chemiluminescent HRP substrate (Merck, Millipore, United States); streptozotocin (Enzo Life
106 Sciences, Germany); Oil Red O (Sigma–Aldrich, Germany); Accu-Chek test strips, Accu-Check
107 glucometer, and protease inhibitor cocktail (Roche Diagnostics, Germany); albumin fraction V,
108 hematoxylin Gill II, acrylamide, and agarose (Carl ROTH, Germany); aqueous mounting medium
109 (ZYTOMED, Germany); "high-fat diet" (HFD) experimental food (Western-type diet containing
110 21% fat and 0.21% cholesterol or Paigen diet containing 16% fat, 1.25% cholesterol (TD88137,
111 Ssniff, Germany), and 0.5% sodium cholate, (D12336, Ssniff, Germany); PBS (Life Technologies,
112 Germany); rompun 2% (Bayer, Germany); and ketamine 10% (beta-pharm, Germany).

113

114 **Mice**

115 Eight-week-old male LDLR$^{-/-}$ (002207) mice were obtained from the Jackson Laboratory (Bar
116 Harbor, ME, USA). Male wild-type C57BL/6N mice were obtained from Charles River
117 Laboratories (Wilmington, MA, USA). Only age-matched male mice were used throughout the
118 study (6-7 mice per group). All animal experiments complied with the ARRIVE guidelines and
119 were carried out in accordance with the Directive 2010/63/EU guidelines. They were conducted
120 following standards and procedures approved by the local Animal Care and Use Committee (35-
121 9185.81/G-185/19, Regierungspräsidium Karlsruhe, Germany).

122

123 **Generation and quantification of rAAV8 viral particles**

124 Recombinant rAAV8 vector particles were generated and purified using the iodixanol gradient
125 ultracentrifugation method(9, 10). rAAV8 production was carried out using HEK293T cells. First,
126 1.8 x 10^8 HEK293T cells were seeded in a ten-chamber CellStack (Corning, USA) and cultured in
127 DMEM+ Glutamax (Gibco, Thermo Fisher Scientific, USA) supplemented with 10% fetal bovine
128 serum (FBS) and 1% penicillin G/streptomycin. After 48 hours, a 1:1:1 molar ratio of pAAV-
129 D377YmPCSK9-bGHpA plasmid(7), the rep-cap AAV8 helper plasmid and an adenoviral helper
130 plasmid was mixed and transfected using polyethylenimine (PEI) (Polyscience, USA). The cells
131 were harvested in 3 ml of lysis buffer and lysed by four freeze–thaw cycles 72 hours after
132 transfection. The vector particles were purified using an iodixanol (Progen, Germany) gradient
133 consisting of four phases with decreasing density (60%, 40%, 25%, and 15%) and
134 ultracentrifugation at 50,000 x g for 135 min at 4 °C. Approximately 3 ml of the 40% phase, in
135 which predominantly full virus particles accumulated, was recovered with a 27G needle. Finally,
136 the vector solution was buffered into PBS using dialysis tubes (Zeba Spin Desalting Columns 7K
137 MWCO, Thermo Scientific, USA) and concentrated (VivaSpin 10K MWCO, Sartorius, Germany).
138 The vector titer was quantified as genome copy numbers per milliliter using a qPCR SYBR-Green
139 assay (Bio–Rad) and primer sequences specific for the bGHpA sequence (bGHpA-fw

140 5´ACCTAACTCACTGATCCGAAATTA 3´, bGHpA-rev 5´ATTTCGGATCAGTGAGTTAGG
141 3´)(11).

142

143 **Induction of atherosclerosis by hypercholesterolemia (HCi) and hypercholesterolemia and**
144 **hyperglycemia (HGHCi) in mice**

145 Adeno-associated viral vectors encoding the gain-of-function variant D377Y of murine PCSK9
146 (rAAV8-PCSK9^{D377Y}) under the control of a liver-specific promoter were delivered via a single
147 retro-orbital sinus injection (1.0 x 10^{11} viral genomes/mouse), and treated animals were fed either
148 a high-fat Western-type diet (HFD, containing 21% fat and 0.21% cholesterol) or a high-
149 cholesterol/high-fat Paigen diet (PD, containing 16% fat, 1.25% cholesterol, and 0.5% sodium
150 cholate) to induce chronic hypercholesterolemia (HCi). Control animals not treated with rAAV8-
151 PCSK9^{D377Y} were fed a high-fat diet (graphic abstract).

152 To induce chronic hyperglycemia and hypercholesterolemia (HGHCi), mice were injected with
153 streptozotocin (STZ, 60 mg/kg, intraperitoneally, once daily for five consecutive days, freshly
154 dissolved in 0.05 M sterile sodium citrate, pH 4.5) one week after rAAV8-PCSK9^{D377Y} application.
155 As a control for STZ injections, mice received injections with an equal volume of 0.05 M sodium
156 citrate, pH 4.5, for 5 days. As PCSK9 expression leads to the degradation of low-density lipoprotein
157 (LDL) receptors, we quantitatively compared the development of atherosclerotic plaque formation
158 in the inducible HCi and HGHCi models with that in LDLR$^{-/-}$ mice fed a HFD or PD. LDLR$^{-/-}$ mice
159 served as the established control model for hypercholesterolemia-evoked atherosclerosis(12).
160 Blood glucose levels were monitored twice a week using the Accu-Chek Aviva system (Roche,
161 USA) and maintained in the range of 300–500 mg/dl. Body weight was measured once weekly.
162 HFD and/or hyperglycemia (minimum 300 mg/dl) was maintained for up to 12 or 20 weeks. In the
163 first 4 weeks of the study, some mice in the PD and HFD groups did not tolerate the food. These
164 animals showed a strong reduction in body weight, which was defined as a termination criterion.
165 Consequently, these mice were removed from the study. Mice fed the PD were analyzed after 8-9
166 weeks due to early mortality in the hyperglycemic group (**Supplementary Figure I**). At the
167 respective study endpoints, mice were sacrificed, and atherosclerotic plaque morphology was
168 analyzed as previously described(13–15).

169

170 **Analysis of mice**

171 At the end of the study period (12 or 20 weeks for HFD or 8 weeks for PD), body weight was
172 measured, and the mice were sacrificed(14–16). Blood samples were obtained from the inferior
173 vena cava of anticoagulated mice (500 U of unfractionated heparin, intraperitoneally). Blood was
174 centrifuged at 2,000 x g for 20 min at 4 °C, and plasma was snap frozen in liquid nitrogen. Mice
175 were perfused with ice-cold PBS for 10 min, and the heart and aortic arches, including the
176 brachiocephalic arteries, were embedded in O.C.T. compound and snap frozen. Brachiocephalic
177 arteries (from distal to proximal) and upper hearts (aortic sinus) were sectioned at 5- and 10-µm
178 thickness, respectively.

179 **Plasma analysis**

180 Heparin plasma was prepared for the measurement of plasma lipids. A total of 500–700 µl of blood
181 per mouse was collected in heparin tubes and centrifuged at 3,500 x g for 10 min at room
182 temperature. Plasma was transferred to a 1.5-ml tube and stored at -80 °C. Plasma samples of HFD-
183 and PD-fed mice were diluted 1:5 with 0.9% NaCl before cholesterol and triglyceride
184 measurements. Plasma samples were analyzed in the accredited central laboratory of Heidelberg
185 University Hospital using standard operating procedures according to the manufacturers'
186 instructions. Cholesterol and triglycerides were analyzed on a Siemens ADVIA Chemistry XPT
187 System (reagent kits 04993681 and 10697575, respectively). We measured the concentrations of
188 mouse IL-1β by ELISA (R&D Systems) according to the manufacturer's instructions.

189

190 **Histology**

191 Oil Red O staining was conducted on frozen cross-sections of the aortic sinus and the truncus of
192 the brachiocephalic artery (BCA) (14, 17). Cryopreserved cross-sections of the brachiocephalic
193 arteries and aortic sinus (5 and 10 µm, respectively) were fixed in ice-cold acetone for 2 min, rinsed
194 twice in ice-cold 1x PBS, and stained with Oil Red O for 10 min. Sections were rinsed twice with
195 distilled water for 20 seconds and once in running tap water for 10 min. Sections were then
196 counterstained with hematoxylin for 40 seconds, rinsed in tap water, and mounted with aqueous
197 mounting medium. Movat staining was performed on frozen sections of the aortic sinus and
198 brachiocephalic arteries. Frozen sections (5 µm) were fixed in Bouin's solution at 50 °C for 10 min
199 and stained with 5% sodium thiosulfate for 5 min, 1% alcian blue for 15 min, alkaline alcohol for
200 10 min, Movat's Weigert's solution for 20 min, crocein scarlet acid/fuchsin solution for 1 min, 5%
201 phosphotungstic acid for 5 min and 1% acetic acid for 5 min. Between every staining step, the
202 tissue sections were washed with tap water and distilled water. Sections were then covered with
203 cytoseal mounting medium. Every 15th section (~90 µm) of the brachiocephalic arteries and aortic
204 sinus were analyzed to quantify the plaque area. The following parameters were determined. 1)
205 The vessel lumen, where the vessel lumen is the area within the blood vessel, consisting of both
206 the remaining open lumen and the plaque area, that does not include the vessel wall itself. 2) Total
207 plaque size, where the size of the plaque comprises all parts of the atheroscleroma (fibrous cap,
208 necrotic tissue, fibrous tissue, etc.) within the vessel lumen. 3) The necrotic core (as a percentage)
209 is defined as the area stained blue upon Movat's pentachrome staining and is presented as the
210 percentage of the total plaque size. 4) The fibrous cap, which is the minimal thickness of the fibrous
211 tissue overlaying the necrotic core. If multiple necrotic cores were present within one plaque, the
212 thickness of all fibrous caps was determined, and the average was used for further analyses. 5) the
213 EEL, IEL and media, where the area surrounded by the external elastic lamina (EEL) and the
214 internal elastic lamina (IEL) were measured using bright field images of Oil Red O-stained BCA
215 images as described previously (18) (**Supplementary Figure II**). The EEL and IEL were encircled
216 (**Supplementary Figure II**), and their areas were measured using Image-Pro Plus software. The
217 media area was calculated by subtracting the IEL area from the EEL area. The lumen area was
218 calculated by subtracting the plaque area from the IEL area. Thickness was measured using ImageJ

219 software using a free-hand tool (13, 14). Cryosections of PD-fed mice were used for picrosirius red
220 staining (Sigma–Aldrich, Germany) according to the manufacturer's instructions. Tissue sections
221 were then stained with picrosirius red solution for 1 h at room temperature. The sections were
222 washed 2 times in acidified water (5 ml of glacial acetic acid to 1 liter of water) and mounted. For
223 histological analysis, images were captured with a Keyence BZ-X810 fluorescence microscope
224 (aortic sinus) and an Olympus Bx43 microscope (brachiocephalic arteries). Image-Pro Plus
225 software (version 6.0) and ImageJ software were used for image analysis(14, 15, 17).

226

227 **Immunohistochemistry and immunofluorescence staining**

228 For immunohistochemistry and immunofluorescence staining, frozen sections of brachiocephalic
229 arteries (BCA) and aortic roots were fixed in ice-cold acetone for 8 min, washed twice with ice-cold
230 PBS and incubated in 2% BSA in PBST for 1 h. Sections were then incubated overnight at 4 °C with
231 primary antibodies against α-SMA (1:250) and CD68 (1:1000). Sections incubated without primary
232 antibodies were used as negative controls for background correction. After overnight incubation, the
233 sections were washed three times with PBS followed by incubation with corresponding horseradish
234 peroxidase (HRP)-labeled secondary antibodies. After washing, tissues were counterstained using
235 3,3'-diaminobenzidine (DAB)/hematoxylin. Primary antibody against MOMA-2 (1:100) was
236 incubated overnight at 4 °C, followed by washing three times with PBS and incubation with
237 fluorescently labeled corresponding secondary antibody. Sections incubated without secondary
238 antibody were used as negative controls and for background correction. After washing, nuclear
239 counterstaining was conducted using mounting medium with DAPI. Images were captured and
240 analyzed using a Keyence BZ-X810 all-in-one fluorescence microscope and an Olympus Bx43
241 microscope (Olympus, Hamburg, Germany) using the same settings in the experimental and control
242 groups. Analyses were performed by two independent blinded investigators. ImageJ software
243 (Version 1.8.0) was used for image analysis.

244

245 **Immunoblotting**

246 Proteins were isolated, and immunoblotting was performed as previously described(19). Mouse
247 livers were weighed, and an adjusted volume of RIPA buffer containing protease inhibitor cocktail
248 (100 µl/10 mg) was added. Tissue was homogenized mechanically using 20G and 25G needles
249 followed by a 30-min incubation on ice with sequential vortexing. Samples were centrifuged at
250 12,000 x g for 20 min at 4 °C. The supernatant was transferred to a fresh tube, and the protein
251 concentration was determined using the Pierce™ BCA Protein Assay Kit following the
252 manufacturer's instructions and a Varioskan Lux plate reader (Thermo Fisher Scientific, Waltham,
253 MA, USA). Samples were separated using the Mini-PROTEAN® TGX™ Precast Gel 4-15% (Bio–
254 Rad Laboratories, Inc., Hercules CA, USA) and transferred to a nitrocellulose membrane.
255 Membranes were incubated with Invitrogen No-Stain solution for 10 min and blocked for 1 h in 5%
256 low-fat milk dissolved in TBS-T. Incubation with primary anti-mLDLR antibody and anti-β-actin
257 was performed overnight at 4 °C. Membranes were incubated with the corresponding secondary

258 rabbit anti-goat immunoglobulin/HRP and goat anti-mouse immunoglobulin/HRP for 1 h at room
259 temperature. Millipore Immobilon Classico Western HRP Substrate was applied to detect the signal
260 using iBright 1500 (Thermo Fisher Scientific, Waltham, MA, USA). Densiometric analysis was
261 performed using ImageJ software.

262

263 **RNA-seq, functional annotation and pathway analysis**

264 RNA was extracted from aortic tissues (comprising the plaque and surrounding tissue) using an
265 RNeasy mini kit (QIAGEN, Germany), and the RNA concentration was measured using a
266 Nanodrop (2000C, Peq lab, Germany). The quality and integrity of RNA were controlled with an
267 Agilent Technologies 2100 Bioanalyzer (Agilent Technologies, Waldbronn, Germany). Expression
268 profiling was performed using RNA sequencing (RNA-seq). An RNA sequencing library was
269 generated from 500 ng of total RNA using a Dynabeads® mRNA DIRECT(tm) Micro Purification
270 Kit (Thermo Fisher) for mRNA purification followed by a NEBNext® Ultra(tm) II Directional
271 RNA Library Prep Kit (New England BioLabs) according to the manufacturer's protocols. The
272 libraries were sequenced on an Illumina NovaSeq 6000 using a NovaSeq 6000 S2 Reagent Kit (100
273 cycles, paired-end run) with an average of 3 x 10^7 reads per RNA sample. A quality report was
274 generated by the FASTQC (version 0.11.8) tool for each FASTQ file. Before alignment to the
275 reference genome, each sequence in the raw FASTQ files was trimmed on base call quality and
276 sequencing adapter contamination using the Trim Galore! wrapper tool (version 0.4.4). Reads
277 shorter than 20 bp were removed from the FASTQ file. Trimmed reads were aligned to the
278 reference genome using the open source short read aligner STAR (version 2.5.2b,
279 https://code.google.com/p/rna-star/) with settings according to the log file. Feature counts were
280 determined using the R package Rsubread (version 1.32.4). Only genes showing counts greater
281 than 5 at least two times across all samples were considered for further analysis (data cleansing).
282 Gene annotation was performed using the R package bioMaRt (version 2.38.0). Before starting the
283 statistical analysis steps, expression data were log2 transformed and normalized according to the
284 50th percentile (quartile normalization using edgeR, version 3.24.3). Differential gene expression
285 was calculated by the R package edgeR. Statistically significant DEGs ($p<0.05$ and FDR <0.05)
286 were sorted and categorized after correcting for multiple hypothesis testing by the Benjamini–
287 Hochberg method. The threshold to identify differentially expressed genes (DEGs) was set to a
288 logFc value of ± 0.58 (IRI group), resulting in a 1.5-fold expression change. To identify genes
289 differentially regulated by either hyperlipidemia (HCi) or combined hyperglycemia and
290 hyperlipidemia (HGHCi), DEGs between the HFD (control) group and either group were identified
291 based on a minimum logFc difference value of ±0.58. Heatmapper (http://www.heatmapper.ca/)
292 was used to generate heatmaps of gene expression data. Genes shown in the heatmap were sorted
293 based on DEGs in the control group (HFD without PCSK9 injections) based on their log Fc values.
294 For representation purposes, no clustering method was applied, and the z score was used. Venny
295 (version 2.1), an online interactive tool, was used for comparison and identification of overlapping
296 DEGs between different groups. Gene ontology was performed using the online tool Database for
297 Annotation, Visualization and Integrated Discovery (DAVID) version 6.8 bioinformatics package,

298 and Benjamini Hochberg adjustment was applied to all enriched p values to control for multiple
299 testing. All RNA-seq analyses were performed by an independent blinded investigator.

300

301 **qPCR analysis**

302 RNA was isolated using an RNeasy Mini kit from Qiagen, and reverse transcription was performed
303 with iScript (Bio–Rad) Mastermix. Primer sequences and probes are listed in the Major Resources
304 Table in the Supplemental Material. qPCR analyses were performed with PowerUp SYBR Green
305 Mastermix (Thermo Fisher). All samples were run in duplicate, and relative gene expression was
306 converted using the 2-ΔΔCT method against the mean of two internal control housekeeping genes,
307 namely, hypoxanthine-guanine phosphoribosyl transferase (*Hprt*) and β-2 Microglobulin (*B2m*) for
308 mice. ΔΔCT= (CTexperiment gene – CTmean experiment housekeeping) - (CTcontrol gene –
309 CTmean control housekeeping). The relative gene expression in the control HFD group was set at
310 1.

311

312 **Statistical analysis**

313 Statistical analyses were performed with GraphPad Prism (version 7; GraphPad Software Inc., La
314 Jolla, CA, USA). The significance level was set at $p< 0.05$ for all comparisons. The data are
315 summarized as the mean ± standard error of the mean (SEM). Comparisons of two groups were
316 analyzed with unpaired Student's T test. Statistical analyses of more than two groups were
317 performed with analysis of variance (ANOVA) and Sidak's post hoc comparisons. Differences
318 between groups of a single independent variable were determined using one-way ANOVA, and
319 between two independent variables using two-way ANOVA. The Kolmogorov–Smirnov test or
320 D'Agostino-Pearson normality test was used to determine whether the data were consistent with a
321 Gaussian distribution.

322

323 ## Results

324 **The combination of hyperglycemia and hyperlipidemia exacerbates atherosclerosis in**
325 **PCSK9^{D377Y}-expressing mice fed a high-fat diet**

326 To induce hypercholesterolemia (HCi), 8-week-old C57BL/6N mice were administered a single
327 dose of rAAV8-PCSK9^{D377Y} (1.0 x 10^{11} adeno-associated viral particles, intravenously) one week
328 before feeding a high-fat diet (HFD, Western-type diet). Saline-injected mice fed a HFD served as
329 a control for rAAV8-PCSK9^{D377Y} intervention (control HFD). Saline-injected mice with genetic
330 deficiency of low-density lipoprotein receptor (LDLR knockout (KO)) on a HFD served as controls
331 for rAAV8-PCSK9^{D377Y} treatment (**Figure 1A**). The mouse group in which hypercholesterolemia
332 evoked by PCSK9 expression and HFD (HCi, single hit) was combined with induction of chronic
333 hyperglycemia using STZ injection (double hit) is hereafter termed HGHCi (high glucose high
334 cholesterol - inducible) throughout the manuscript. For quantification of atherosclerotic plaque

335 formation, mice were euthanized 12 (early time point) or 20 (late time point) weeks after rAAV8-
336 PCSK9^{D377Y} injection and the start of HFD feeding.

337 As anticipated, rAAV8-PCSK9^{D377Y} administration resulted in a strong reduction in hepatic LDL
338 receptor protein levels compared with saline-injected mice after both 12 and 20 weeks of
339 intervention (**Figure 1B, C**). All mice thrived well, and body weight (**Supplementary Table 1**),
340 blood lipids and glucose levels differed among treatment groups (**Figure 1D-E**). Plasma
341 cholesterol levels were higher in the HGHCi HFD group than in the HCi HFD animals both at the
342 early and late time points (**Figure 1D**); however, plasma triglyceride levels were higher in the
343 HGHCi HFD vs. HCi HFD group only after 20 weeks (**Figure 1F**). Plasma triglyceride, cholesterol
344 and glucose levels were comparable between rAAV8-PCSK9^{D377Y} (HCi HFD group) and LDLR
345 KO mice on a HFD (**Figure 1D-F**).

346 Analyses of hematoxylin and eosin (H&E)- and Oil Red O-stained aortic root sections as well as
347 the assessment of the aortic plaque score (**Supplementary Figure III A**) showed larger
348 atherosclerotic plaques at both vascular sites (aortic sinus and BCA) in HGHCi HFD mice than in
349 HCi HFD mice, both at early and late time points (aortic sinus at 12 weeks: HCi HFD 16% vs.
350 HGHCi HFD 37% plaque area; 20 weeks: HCi HFD 29% vs. HGHCi HFD 43% plaque area)
351 (**Figure 2A-D**). Control HFD mice had no lesions, whereas all rAAV8-PCSK9^{D377Y}-injected mice
352 on HFD (HCi HFD group) developed atherosclerosis to a similar extent as LDLR KO mice on HFD
353 after 12 weeks and with no significant difference after 20 weeks (**Figure 2A-I**). In addition, HGHCi
354 mice on a HFD had larger Oil Red O-stained plaques in the aortic sinus than LDLR KO HFD mice
355 at both time points (**Figure 2C, D**). There was no significant difference in atherosclerotic plaque
356 size between HGHCi HFD and LDLR KO HFD (**Figure 2E, F**) in the truncus brachiocephalic
357 artery (BCA). In contrast to the aortic sinus, we found no significantly increased lesion area in the
358 truncus brachiocephalic artery at 12 weeks, suggesting that the lesion develops earlier in the aortic
359 sinus than in the brachiocephalic artery (**Figure 2E, F**). Image analysis of cross sections of BCA
360 revealed a comparable EEL and IEL-area in HCi HFD and LDLR HFD mice, but thicker media
361 and reduced lumen area in LDLR HFD mice (**Figure 2G-J**), the latter in line with increased plaque
362 size in BCA of the LDLR HFD group (**Figure 2E, F**). In HGHCi HFD mice, EEL, IEL, media,
363 and lumen area were reduced at 12 weeks compared with the HCi-HFD group. After 20 weeks, a
364 reduction in lumen area persisted in HGHCi HFD mice compared with HCi HFD mice (**Figure
365 2J**), whereas EEL, IEL and media were comparable between the two groups (**Figure 2G-I**).

366

367 **Less stable plaque phenotypes in hyperglycemia and hyperlipidemia (HGHCi) versus
368 hyperlipidemic (HCi) mice**

369 In addition to plaque size, plaque stability is an important determinant of clinical outcome. We
370 therefore evaluated indirect parameters of plaque stability in HCi, HGHCi and LDLR KO mice.
371 Indeed, signs of plaque instability were more pronounced in HGHCi HFD mice than in HCi HFD
372 mice, as evidenced from an increased necrotic core area, thinner fibrous caps, and reduced
373 intraplaque α-SMA-positive cells, while no changes in the total vessel lumen were observed
374 (**Figure 3A-J, Supplementary Figure IIIB**). Measurement of indirect markers of plaque stability

375 was analyzed in Movat pentachrome-stained cross-sections of the aortic sinus (**Figure 3A-C**) and
376 truncus brachiocephalic artery (**Figure 3D-F**). While HCi HFD and LDLR KO HFD mice
377 developed few atherosclerotic lesions with increased necrotic core areas in the aortic sinus at 12
378 weeks (Figure 3A), diabetic HGHCi HFD mice showed increased necrotic core areas at this early
379 time point. At 20 weeks, diabetic HGHCi HFD mice had significantly increased necrotic core areas
380 and thinner fibrous caps at both vascular sites (aortic sinus and truncus brachiocephalic artery)
381 compared to HCi HFD and LDLR KO HFD mice (**Figure 3A-F**). Plaque morphology and stability
382 depend in part on the cellular composition of plaques. After 20 weeks, the number of α-SMA-
383 positive cells within plaques of the aortic sinus and truncus brachiocephalic artery of HGHCi HFD
384 mice was significantly decreased compared to that of nondiabetic HCi HFD mice but not of LDLR
385 KO HFD mice (**Figure 3H, J**). There was no difference in α-SMA in the aortic sinus between
386 HGHCi HFD and HCi HFD and LDLR KO mice after 12 weeks (**Figure 3G, H**). In the truncus
387 brachiocephalic artery, HCi HFD mice showed no increased plaque development at 12 weeks, and
388 accordingly, the number of α-SMA-positive cells was very low in this group (**Figure 3I, J**).
389 However, in all other groups (HGHCi and LDLR KO at 12 weeks and HCi, HGHCi, and LDLR
390 KO at 20 weeks), the number of α-SMA-positive cells within plaques was significantly increased
391 compared to the control group in BCA (**Figure 3I, J**). Furthermore, we investigated intraplaque
392 hemorrhage (by the erythrocyte marker protein Ter-119) in HGHCi HFD mice and found no
393 significant differences between the HCi HFD and HGHCi HFD groups (**Supplementary Figure**
394 **IV**).

395

396 **Increased IL-1β plasma levels and expression of proinflammatory markers in hyperlipidemic**
397 **and hyperglycemic mice compared to hyperlipidemic mice**

398 As atherosclerosis is a chronic inflammatory disease and cytokines strongly influence disease
399 development, we measured the plasma level of IL-1β and found significantly increased IL-1β levels
400 in the diabetic HGHCi HFD group (5.8 pg/mL at 12 weeks; 5.6 pg/mL at 20 weeks) compared to
401 the HCi HFD (1.9 pg/mL at 12 weeks; 1.8 pg/mL at 20 weeks) and LDLR KO HFD mice (3.5
402 pg/mL at 12 weeks; 2.6 pg/mL at 20 weeks) at both study time points (**Figure 4A**), indicating that
403 systemic inflammation is already increased during early plaque development. As IL-1β was already
404 increased after 12 weeks in the HGHCi HFD group, we analyzed the expression of marker genes
405 of macrophage polarization (*Cd68* and *iNos* as M1 macrophage polarization marker genes; *Arg1*
406 and *Fizz* as M2 marker genes) in the aorta of 12-week-old mice and found increased expression of
407 M1 macrophage markers (*Cd68* and *iNos*) (**Figure 4B, C**) and correspondingly lower gene
408 expression of M2 macrophage markers (*Arg1* and *Fizz*) (**Figure 4D, E**). In line with these results,
409 the content of MOMA-2-positive cells was increased in plaques of the truncus brachiocephalic
410 artery (BCA) (**Figure 4F, G**) of HGHCi HFD mice. In the aortic sinus, the number of MOMA-2-
411 positive cells was elevated in all groups exhibiting atherosclerosis (HCi, HGHCi, and LDLR KO
412 at 12 and 20 weeks) (**Figure 4H, I**).

413 Taken together, the observed shift toward increased lesion area, inflammation and necrotic core
414 area and reduced fibrous cap thickness and α-SMA content suggests that plaque stability is reduced
415 in HGHCi HFD mice compared to HCi HFD mice(20, 21).

416

417 **Identification of HGHCi-specific transcriptional responses in the aorta**

418 We next aimed to identify transcriptional signatures that are engaged in the vasculature by
419 combining chronic hyperlipidemia and hyperglycemia to generate hypotheses about signaling
420 pathways contributing to larger but unstable plaques in HGHCi HFD mice. To this end, we
421 conducted unbiased gene expression analyses (RNAseq) in the cohorts of control HFD, HCi HFD
422 and HGHCi HFD mice at 12 weeks. In aortic tissue of HCi HFD mice, the expression of 942 genes
423 was induced compared to the control mice solely on a HFD (**Figure 5A**). Conversely, gene
424 expression in the aorta of HGHCi HFD mice was strikingly different from that of HCi HFD mice.
425 Gene expression of a large set of genes was dysregulated in HGHCi HFD mice. Thus, in aortic
426 tissue of HGHCi HFD mice, the expression of 2759 genes was induced compared to aortic samples
427 of saline-treated HFD-fed mice (control HFD) (**Figure 5A**). A total of 418 genes showed similar
428 expression in both HGHCi HFD and HCi HFD mice, and differential regulation of 2341 genes
429 could be specifically assigned to combined hyperglycemia and hyperlipidemia.

430 We next performed functional annotation analysis to study the gene pathways that are specifically
431 engaged in the vessels of the HGHCi HFD group and observed that combined hyperglycemia plus
432 hyperlipidemia led to significant changes in the expression of genes encoding signaling molecules
433 involved in inflammation, intracellular lipid transport, cholesterol metabolic processes,
434 extracellular matrix (ECM) degradation, and cellular metabolism (**Figure 5B**). We further
435 performed gene ontology analysis on genes that were induced in aortic tissue of HCi HFD and
436 HGHCi HFD mice. Gene ontology analysis of differentially expressed genes revealed that
437 combined hyperglycemia and hyperlipidemia led to the upregulation of genes involved in the
438 inflammatory response (GO:0006954) (**Figure 5C**) and ECM degradation (GO:0030198) (**Figure
439 5F**). We further investigated the expression of TNFa, which is a central mediator of inflammatory
440 reactions and plays an important role in atherogenesis, and found that it was significantly
441 upregulated in the HGHCi HFD mice compared to HCi HFD mice at both study time points (**Figure
442 5D, E**). Moreover, we analyzed additional matrix metalloproteinases, such as Mmp14 and Adamts4
443 (A Disintegrin and Metalloproteinase with Thrombospondin motifs 4), in the RNA-seq data and
444 corroborated their dysregulation by qPCR analysis (**Figure 5G-J**). Both marker genes were
445 upregulated in HGHCi HFD mice compared to HCi HFD mice after both 12 and 20 weeks (**Figure
446 5G-J**).

447

448 **The Paigen diet accentuates atherosclerosis and promotes plaque instability in mice with
449 combined hyperglycemia and hyperlipidemia**

450 We next tested the atherosclerosis model following induction of combined hyperglycemia and
451 hyperlipidemia (HGHCi) in mice fed a Paigen diet (PD), which leads to higher plasma cholesterol

452 levels (7) and might thus further exacerbate the formation of atherosclerotic plaques. PD-fed mice
453 were treated with the same batch and dose of rAAV8-PCSK9^{D377Y}, and LDLR KO mice on the PD
454 served as a reference for comparison. Saline-injected mice fed the PD served as a control for
455 rAAV8-PCSK9^{D377Y} intervention. Hyperlipidemic and hyperlipidemic plus hyperglycemic mice
456 on the PD are hereafter called HCi PD and HGHCi PD mice, respectively, for simplicity. In HGHCi
457 PD mice, we observed an increased mortality (25% in week 8, i.e., 5 out of 20 mice died in this
458 group (**Supplementary Figure I, A**). Based on these incidences, it was decided that the remaining
459 animals in this group should be sacrificed and analyzed 8-9 weeks after induction of combined
460 hypercholesterolemia and hyperglycemia, since the 12- and 20-week time points chosen for the
461 HGHCi group on HFD might not have been reached. Thus, mice from all groups on the PD diet
462 were euthanized 8-9 weeks after rAAV8-PCSK9^{D377Y} injection to quantify atherosclerosis (**Figure**
463 **6A**). Hepatic LDL receptor protein expression was already abrogated at this time point compared
464 with saline-injected mice (control PD) (**Figure 6B, C**). As expected, body weight (**Supplementary**
465 **Table 1)**, plasma cholesterol levels and blood glucose levels differed among the HCi and HGHCi
466 PD groups (**Figure 6D-F),** while HCi PD mice and LDLR KO PD mice did not differ regarding
467 cholesterol, triglyceride and glucose levels (**Figure 6D-F**). In a preliminary pilot study, we
468 compared the plasma cholesterol levels of the HGHCi PD group with STZ-treated mice (STZ PD)
469 and citrate-treated controls (citrate PD) fed a Paigen diet (**Supplementary Figure V**). Notably,
470 mice with STZ-evoked hyperglycemia and on a high-cholesterol, high-fat Paigen diet (without
471 AAV-mPCSK9 treatment) did not exhibit an increase in plasma cholesterol (**Supplementary**
472 **Figure IV).** Application of the Paigen diet exacerbated atherosclerosis in both HGHCi PD and HCi
473 PD mice compared to the corresponding groups on the HFD diet ($p< 0.05$). Interestingly, the aortic
474 root plaque sizes of HGHCi PD and HCi PD mice at 8 weeks (**Figure 6G-J)** were comparable to
475 those of HGHCi and HCi mice on a HFD at 20 weeks (**Figure 2A**). Consistent with data from the
476 HFD groups, signs of plaque instability were more pronounced in HGHCi PD mice than in HCi-
477 PD mice as measured by decreased collagen deposition (picrosirius red staining) and increased
478 plaque CD68-positive cells in HGHCi PD mice in comparison with HCi PD mice (**Figure 7A-D**).
479 Taken together, these data suggest that the PD aggravates atherosclerosis in mice and shows plaque
480 formation after 8 weeks, therefore representing a direct inducible diabetic atherosclerosis model
481 with more aggravated atherosclerosis than HGHCi HFD.

482

483 ## Discussion

484 The most frequently used models to study diabetes mellitus-associated atherosclerosis in mice rely
485 on genetically modified models. Thus, mouse studies evaluating diabetes-associated
486 atherosclerosis rely on ApoE$^{-/-}$ or LDLR$^{-/-}$ mice, where hypercholesterolemia is combined with
487 chronic hyperglycemia following beta-cell destruction by injection of streptozotocin (STZ) or viral
488 infection (22) or by crossbreeding with mouse strains carrying a point mutation in the gene
489 encoding insulin leading to a misfolding of the proinsulin 2 protein (Ins2^{+}/Akita) (4, 23). Induction
490 of hyperglycemia with STZ led to higher plasma cholesterol levels and showed significant
491 acceleration of atherosclerotic lesion formation in ApoE$^{-/-}$ and LDLR$^{-/-}$ mice compared to

492 nondiabetic ApoE$^{-/-}$ and LDLR$^{-/-}$ controls (6, 24–30). Additionally, the severe hyperglycemia in
493 Ins2^{+}/Akita mice crossbred with ApoE$^{-/-}$ and LDLR$^{-/-}$ leads to a pronounced increase in
494 atherosclerosis and non-HDL cholesterol and triglyceride levels compared to those of
495 nonhyperglycemic control mice (4, 31, 32). Although these genetic models are useful tools for
496 studying diabetic complications, intensive crossbreeding of these mouse lines is required. This
497 becomes even more laborious and time-consuming when diabetic long-term complications are to
498 be induced in knockout mouse lines for evaluation of the causal role of the gene of interest under
499 certain metabolic conditions. Concomitant induction of both hypercholesterolemia and
500 hyperglycemia at discrete time points in a given mouse line has not been reported.

501 Here, we describe a novel strategy to induce an atherosclerosis model aggravated by concomitant
502 induction of hyperglycemia without the necessity of genetic germline engineering but via rAAV8-
503 mediated gene transfer of mutant PCSK9^{D377Y} in hepatocytes in combination with STZ-evoked
504 beta-cell destruction (HGHCi). Comparison of plasma cholesterol levels shows increased
505 cholesterol levels in the HCi model, which increase further by additional induction of
506 hyperglycemia in the HGHCi model. The additional increase in cholesterol levels is a consequence
507 of the two-hit model because induction of hyperglycemia alone does not increase plasma
508 cholesterol levels. The increased plasma cholesterol levels in the diabetic mice (HGHCi group) are
509 part of the phenotype of our model and resemble findings in previous studies (7,26,28,29).
510 Dyslipidemia aggravated by hyperglycemia is independent of whether the diabetes was induced by
511 STZ injection or genetically (e.g., InsAkita mutant mice). Increased cholesterol levels in the
512 diabetic mice most likely reflect decreased lipoprotein clearance, and as such, they may reflect an
513 important feature of diabetes-associated dyslipidemia. Thus, Goldberg et al. demonstrated that the
514 plasma cholesterol levels of STZ-induced diabetic LDLR$^{-/-}$ mice were twice those of nondiabetic
515 control mice. The authors observed an increase in both VLDL and LDL. VLDL in plasma was
516 more enriched in cholesterol, and both VLDL and LDL had high levels of ApoE (30). Further
517 lipidomics analyses are required to define the lipid profile in diabetic and nondiabetic mice with
518 PCSK9^{D377Y}-induced dyslipidemia. We cannot differentiate whether the increased cholesterol level
519 or other factors (e.g., the elevated systemic inflammation) or their combination is responsible for
520 the increased plaque progression in HGHCi mice compared to HCi mice. However, STZ treatment
521 alone did not lead to elevated LDL cholesterol in our study (Supplementary Figure V) or in
522 previous studies (6), where it was shown that diabetic mice are resistant to atherosclerosis even in
523 the presence of a high-fat diet. To address the question of whether the additional increase in LDL
524 cholesterol (evoked by hyperglycemia in PCSK9^{D377Y}-treated mice) is indeed responsible for
525 increased plaque progression, one might design a study using a selective LDL-lowering therapy
526 without an effect on hyperglycemia (e.g., by HMG-CoA reductase inhibitors) in the HGHCi model.
527 The influence of systemic inflammation on increased plaque progression in the HGHCi group
528 compared to the HCi group could be investigated with an anti-inflammatory therapy (e.g., by the
529 anti-IL-1β antibody canakinumab). Studies addressing such mechanistic links will be required in
530 the future.

531 Furthermore, we show that combined hyperlipidemia and hyperglycemia led to a significant
532 enhancement of atherosclerotic plaque formation compared to mice in which hypercholesterolemia

533 was induced without hyperglycemia (HCi). The HCi model in rAAV8-mediated mutant
534 PCSK9^{D377Y}-expressing mice leads to downregulation of hepatic LDL receptor expression and the
535 development of atherosclerotic lesions. The lesion phenotypes closely resemble those in the
536 established LDL-receptor knockout mouse model. Mice in the HGHCi treatment group displayed
537 larger plaques than norrmoglycemic HCi mice on the same diet and LDLR knockout mice (after
538 12 weeks). Treatment-induced systemic atherosclerosis (e.g., in the aortic sinus and in the
539 brachiocephalic artery) and inflammation were measured by increased plasma levels of IL-1β. The
540 plaque phenotypes induced by HGHCi compared to HCi mice are characterized by increased
541 necrotic core area and decreased fibrous cap thickness. Plaques are characterized by increased gene
542 expression of M1 macrophage markers and MOMA-2-positive cells as well as a reduced number
543 of α-SMA-positive cells (at 20 weeks). A comparably increased amount of α-SMA-positive cells
544 was observed in HGHCi HFD and LDLR KO HFD mice at 12 weeks in the aortic sinus and BCA,
545 which is characteristic of early lesion development (33, 34). In HCi HFD mice, the number of α-
546 SMA-positive cells was also increased in the aortic sinus after 12 weeks but not in the BCA, where
547 a small plaque size was observed at that time point. The reason for these differences in plaque size
548 and α-SMA-positive cell content between the aortic sinus and BCA in HCi mice after 12 weeks
549 can be explained by an earlier development of lesions at the aortic sinus, which has been described
550 in other studies (35–37). Whether the earlier onset of α-SMA-positive cell proliferation and
551 migration in the BCA of HGHCi HFD and LDLR KO mice is due to stronger systemic
552 inflammation indicated by the higher increase in IL-1β levels compared with HCi HFD mice at 12
553 weeks needs to be investigated in future studies. Taken together, these data show that the novel
554 HGHCi model provides an overview of plaque development and progression at two locations in
555 the aorta to study interventions aiming to improve plaque size and, importantly, plaque stability.
556 A similar severity of atherosclerosis was observed with the Paigen diet, albeit much earlier, at 8
557 weeks post-intervention initiation, compared to 20 weeks with the HFD. It has been reported that
558 the addition of cholate in combination with a high cholesterol and high fat content in the Paigen
559 diet boosts hypercholesterolemia by facilitating fat and cholesterol absorption, resulting in very
560 early fatty streak lesions in the aortic root and proximal aorta in C57BL/6 mice (38). Thus, our
561 findings are in line with previous work in genetic models, demonstrating that hyperglycemia
562 promotes unstable plaques in both ApoE$^{-/-}$ and LDLR$^{-/-}$ mice (14, 39–41). Our results identify the
563 HGHCi PD model using a Paigen diet as a novel option for specific experimental setups where
564 strong plaque formation and progression are needed at an early time point.

565 Our unbiased gene expression analysis revealed that combined hyperlipidemia and hyperglycemia
566 (HGHCi) dysregulates a large set of genes (i.e., 2341 genes) in the atherosclerotic aorta compared
567 to hyperlipidemia alone (HCi). The aortic tissue gene expression profile of HGHCi mice fed a HFD
568 differed markedly from HCi HFD mice. Among the pathways that were most prominently affected
569 were the inflammatory response, ECM degradation and metabolism. Upregulated proinflammatory
570 genes, such as *Cx3cl1* (or fractalkine) and *Il18r1*, have been shown to be involved in atherogenesis.
571 *Cx3cl1* is a chemokine and exerts cytotoxic effects on the endothelium. Its membrane-bound form
572 promotes adhesion of rolling leukocytes onto the vessel wall, while in its soluble form, it serves as
573 a potent chemoattractant for CX3CR1-expressing cells. Therefore, it affects the context and

574 stability of the atherosclerotic plaque. Blocking the CX3CL1/CX3CR1 pathway in *in vivo* studies
575 ameliorated the severity of atherosclerosis (42). Il18r1 is a member of the interleukin receptor
576 family and is expressed on T-lymphocytes but also on cell types associated with atherogenesis,
577 such as macrophages, endothelial cells, and smooth muscle cells (43). After binding its ligand IL-
578 18, it leads to the expression of IFNγ via the NF-kB-mediated signaling pathway (44). High
579 expression of IL18R is found in plaque-resident macrophages and endothelial cells in humans (45).

580 The increased expression of genes related to ECM degradation (e.g., *Mmp14* and *Adamts4*) is
581 consistent with previous findings showing that glucose-induced advanced glycation end products
582 (RAGE) mediate modification of the components of the ECM and accelerate atherosclerosis under
583 diabetic conditions (46–49). The ECM degradation genes *Mmp14* and *Adamts4* were shown to play
584 key roles in plaque stability. Loss of *Adamts4* in ApoE KO mice increased plaque stability (50),
585 and ADAMTS4 expression in humans was upregulated during carotid atherosclerotic plaque
586 development. Furthermore, ADAMTS4 serum levels were associated with increased plaque
587 vulnerability (51). Metalloproteinases (MMPs), such as *Mmp14*, play an important role in the
588 pathogenesis of atherosclerosis by participating in vascular remodeling, smooth muscle cell
589 migration, and plaque disruption. Mmp14 is recognized as a prominent member of this family,
590 causes pericellular degradation and has the ability to activate other matrix metalloproteinases. It is
591 further detected at high levels in atherosclerotic plaques (52).
592 Genes involved in inflammation, such as *Tnfa*, *Cd68* and *iNos,* were shown to be upregulated in
593 HGHCi HFD mice compared to HCi HFD mice, which has been described in previous studies
594 where their expression is one of the key drivers in atherosclerosis-associated chronic inflammation
595 in arterial blood vessels (48). The progression of atherosclerosis correlates directly with a local
596 increase in TNF-α production in atherosclerotic plaques and blood (53). The expression data may
597 provide a helpful resource for researchers using this model and suggest that this nongenetic model
598 will be suitable for studying important aspects of the emerging crosstalk between inflammatory
599 signaling, glucose metabolism and lipoprotein metabolism (23, 54–56).
600

601 **Limitations of the study**

602 In this study, only male mice were analyzed. As reported previously, rAAV8-PCSK9^{D377Y}-evoked
603 hypercholesterolemia was 3-fold lower in females than in males (57), and consequently, the extent
604 of atherosclerosis development can be expected to be lower or delayed. To characterize the
605 development of atherosclerosis in our HGHCi model in females, new studies will be required in
606 the future to elucidate sex-specific effects in this model. The aim of the study was to develop and
607 characterize novel models of hyperlipidemia and hyperglycemic-associated atherosclerosis.
608 Plasma lipid levels were not identical between groups. Due to the study design, a cohort with only
609 STZ injection was not included, as hyperglycemia induced by STZ treatment or lymphocytic
610 choriomeningitis virus (LCMV) infection alone is not sufficient to induce atherosclerosis
611 development in mice (29, 39). Hence, conclusions about the impact of isolated hyperglycemia on
612 the atherosclerotic plaque phenotype cannot be drawn from the current study.
613 Atherosclerosis development in mice and humans differs in several parameters, including
614 lipoprotein metabolism. In mice, cholesterol is transported mainly in HDL particles due to a lack

615 of cholesteryl ester transfer protein (CETP) expression, whereas humans show high CETP
616 expression, which results in high LDL cholesterol levels (23). Furthermore, wild-type mice have
617 significantly lower total cholesterol levels than humans, which may explain why they do not
618 develop atherosclerosis under natural conditions. In recent years, atherosclerosis-associated genes
619 have been identified and used to generate genetically modified mouse models that are used in
620 atherosclerosis research. The two most commonly used genetic models in atherosclerosis research
621 are the Apoe-/- and Ldlr-/- models (58, 59). Among other parameters, the models exhibit critical
622 differences in cholesterol and lipid metabolism, which makes their use highly dependent on the
623 scientific question. Apolipoprotein E (apoE) binds to chylomicrons and VLDL in plasma and acts
624 as a ligand that initiates uptake of the remnants via the LDL receptor, thereby removing them from
625 the circulation. Deletion of apoE in Apoe-/- mice results in an increase in cholesterol levels by the
626 accumulation of chylomicrons and VLDL (58). In contrast, in the Ldlr-/- model, deletion of LDLR
627 results in an increase in cholesterol levels by the accumulation of plasma LDL, which is much more
628 comparable to the human situation than the elevation of plasma VLDL in Apoe-/- mice (23).
629 Expression of the rAAV-PCSK9^{D377Y} (7) used in this study leads to increased degradation of
630 LDLR, which is comparable to the deletion of LDLR in the Ldlr-/- model. Additionally, in this
631 inducible model, there is an increase in total cholesterol due to the accumulation of LDL particles,
632 and it was shown by Roche-Molina et al. (60) that the lipoprotein profiles of Ldlr-/- mice and
633 rAAV-PCSK9^{D377Y}-treated animals fed a HFD are very similar. Therefore, both the Ldlr-/- and the
634 inducible rAAV-PCSK9^{D377Y} models are currently most suitable for cholesterol and lipid
635 metabolism studies investigating processes in human atherosclerosis development (23). In addition
636 to their lipoprotein profile, the models also differ from the human disease pattern with respect to
637 the sites at which lesions develop. In humans, disease-relevant plaques develop preferentially in
638 the coronary arteries, carotid arteries and peripheral arteries of the legs and arms, whereas in mouse
639 models, lesions are mainly found in the aortic sinus, aortic arch and brachiocephalic artery (23). In
640 addition, the extent of plaque development in mice is reduced, and large vulnerable plaques are
641 often absent compared to humans; thus, plaque ruptures are rarely observed in genetic mouse
642 models, which in turn occur in humans at advanced stages of atherosclerosis and lead to
643 atherothrombotic vessel occlusions (23, 58, 59).
644 In the future, it may be possible to use the HGHCi model in preclinical animal models that more
645 accurately reflect human lipoprotein metabolism and the development and progression of
646 atherosclerotic lesions in coronary arteries than the already established genetic mouse models. Both
647 STZ-mediated hyperglycemia in pigs and rabbits (61, 62) and PCSK9 gain-of-function
648 overexpression-induced hypercholesterolemia in pigs (63) have been demonstrated to date and, in
649 combination, may achieve further important disease-relevant findings about diabetes-accelerated
650 atherosclerosis and inflammation in humans.
651

652 ## Conclusion

653 We describe a novel nongenetically inducible mouse model using a defined treatment with gain-
654 of-function PCSK9 viral particles, streptozotocin and high-fat diets. The detailed characterization
655 of the plaque phenotypes and the expression analysis indicate that this new experimental approach

can be used to study the clinically important pathogenesis of atherosclerosis in hyperglycemia and hyperlipidemia and can be induced at any given time point to prevent or therapeutically interfere with the development of atherosclerosis under diabetic conditions.

Acknowledgement

We thank Sonja Talmon, Beate Hilbert, Christin Richter, Manuela Ritzal, Anja Barnikol-Oettler, and Kathrin Deneser for excellent technical support. We certify that all persons who have made substantial contributions to the manuscript, but who do not fulfill authorship criteria, are named in the acknowledgments section and have provided the corresponding author with written permission to be named in the manuscript.

Authors contribution

S.G., **K.S.** and **R.M**., interpreted the experimental work and prepared the manuscript. **A.W., R.M., S.G., I.G**. and **D.S.** performed and conducted the in vivo experiments; **S.G., I.G.,** and **C.M.,** performed histological analyses and figure preparation; **J.H., J.B**., and **H.K.** performed RNAseq analysis; **S.A.** and **S.F.** assisted in histology. **B.I.** and **U. L.** interpreted the data and assisted in manuscript preparation. **M.F.** designed the study and assisted in manuscript preparation.

Sources of Funding

This work was supported by grants of the 'Deutsche Forschungsgemeinschaft' (including project S03 of the Collaborative Research Centers (SFB) SFB1118 (MF), and IS-67/5-3, IS-67/8-1, IS-67/11-1, and CRC854/B26 to B.I., SH 849/4-1 to K.S.

Conflict of Interest

none declared.

Data Availability

All data that support the findings of this study are available in this study within the manuscript and/or its supplementary materials.

Supplemental Materials

Supplementary Table 1. Characteristics of mice cohort.

Supplementary Figure I. PD fed HGHCi mice showed higher mortality than HFD fed mice.

Supplementary Figure II. Determination of the external and internal elastic lamina, lumen area and media area.

690 **Supplementary Figure III.** Comparison of aortic plaque score and total vessel lumen area.

691 **Supplementary Figure IV.** Intraplaque hemorrhage is not increased in HGHCi HFD mice.

692 **Supplementary Figure V.** Hyperglycemia alone does not affect plasma cholesterol levels in mice fed a
693 Paigen diet.

694 **Major resources table**
695

696 **REFERENCES**

697 1. Correction to: Heart Disease and Stroke Statistics-2019 Update: A Report From the American Heart
698 Association. *Circulation* (2020) **141**:e33. doi:10.1161/CIR.0000000000000746.
699 2. Raghavan S, Vassy JL, Ho Y-L, Song RJ, Gagnon DR, Cho K, et al. Diabetes Mellitus-Related All-Cause
700 and Cardiovascular Mortality in a National Cohort of Adults. *Journal of the American Heart*
701 *Association* (2019) **8**:e011295. doi:10.1161/JAHA.118.011295.
702 3. Fang M, Wang D, Coresh J, Selvin E. Trends in Diabetes Treatment and Control in U.S. Adults, 1999–
703 2018. *The New England journal of medicine* (2021) **384**:2219–28. doi:10.1056/NEJMsa2032271.
704 4. Jun JY, Ma Z, Segar L. Spontaneously diabetic Ins2+/Akita:apoE-deficient mice exhibit exaggerated
705 hypercholesterolemia and atherosclerosis. *American Journal of Physiology-Endocrinology and*
706 *Metabolism* (2011) **301**:E145-E154. doi:10.1152/ajpendo.00034.2011.
707 5. Voyiaziakis E, Goldberg IJ, Plump AS, Rubin EM, Breslow JL, Huang LS. ApoA-I deficiency causes both
708 hypertriglyceridemia and increased atherosclerosis in human apoB transgenic mice. *Journal of lipid*
709 *research* (1998) **39**:313–21.
710 6. Keren P, George J, Keren G, Harats D. Non-obese diabetic (NOD) mice exhibit an increased cellular
711 immune response to glycated-LDL but are resistant to high fat diet induced atherosclerosis.
712 *Atherosclerosis* (2001) **157**:285–92. doi:10.1016/S0021-9150(00)00685-7.
713 7. Bjorklund MM, Hollensen AK, Hagensen MK, Dagnaes-Hansen F, Christoffersen C, Mikkelsen JG, et
714 al. Induction of atherosclerosis in mice and hamsters without germline genetic engineering.
715 *Circulation research* (2014) **114**:1684–9. doi:10.1161/CIRCRESAHA.114.302937.
716 8. Goettsch C, Hutcheson JD, Hagita S, Rogers MA, Creager MD, Pham T, et al. A single injection of gain-
717 of-function mutant PCSK9 adeno-associated virus vector induces cardiovascular calcification in mice
718 with no genetic modification. *Atherosclerosis* (2016) **251**:109–18.
719 doi:10.1016/j.atherosclerosis.2016.06.011.
720 9. Grieger JC, Choi VW, Samulski RJ. Production and characterization of adeno-associated viral vectors.
721 *Nature protocols* (2006) **1**:1412–28. doi:10.1038/nprot.2006.207.
722 10. Zolotukhin S, Byrne BJ, Mason E, Zolotukhin I, Potter M, Chesnut K, et al. Recombinant adeno-
723 associated virus purification using novel methods improves infectious titer and yield. *Gene Therapy*
724 (1999) **6**:973–85. doi:10.1038/sj.gt.3300938.
725 11. Jungmann A, Leuchs B, Rommelaere J, Katus HA, Müller OJ. Protocol for Efficient Generation and
726 Characterization of Adeno-Associated Viral Vectors. *Human gene therapy methods* (2017) **28**:235–
727 46. doi:10.1089/hgtb.2017.192.
728 12. Ishibashi S, Goldstein JL, Brown MS, Herz J, Burns DK. Massive xanthomatosis and atherosclerosis in
729 cholesterol-fed low density lipoprotein receptor-negative mice. *The Journal of clinical investigation*
730 (1994) **93**:1885–93. doi:10.1172/JCI117179.
731 13. Zhou Q, Bea F, Preusch M, Wang H, Isermann B, Shahzad K, et al. Evaluation of Plaque Stability of
732 Advanced Atherosclerotic Lesions in Apo E-Deficient Mice after Treatment with the Oral Factor Xa
733 Inhibitor Rivaroxaban. *Mediators of Inflammation* (2011) **2011**:432080. doi:10.1155/2011/432080.
734 14. Shahzad K, Gadi I, Nazir S, Al-Dabet M'dM, Kohli S, Bock F, et al. Activated protein C reverses
735 epigenetically sustained $p66^{Shc}$ expression in plaque-associated macrophages in diabetes.
736 *Communications biology* (2018) **1**:104. doi:10.1038/s42003-018-0108-5.

737 15. Seehaus S, Shahzad K, Kashif M, Vinnikov IA, Schiller M, Wang H, et al. Hypercoagulability inhibits
738 monocyte transendothelial migration through protease-activated receptor-1-, phospholipase-Cbeta-
739 , phosphoinositide 3-kinase-, and nitric oxide-dependent signaling in monocytes and promotes
740 plaque stability. *Circulation* (2009) **120**:774–84. doi:10.1161/CIRCULATIONAHA.109.849539.
741 16. Shahzad K, Thati M, Wang H, Kashif M, Wolter J, Ranjan S, et al. Minocycline reduces plaque size in
742 diet induced atherosclerosis via p27(Kip1). *Atherosclerosis* (2011) **219**:74–83.
743 doi:10.1016/j.atherosclerosis.2011.05.041.
744 17. Schuster S, Rubil S, Endres M, Princen HM, Boeckel J-N, Winter K, et al. Anti-PCSK9 antibodies inhibit
745 pro-atherogenic mechanisms in APOE*3Leiden.CETP mice. *Scientific reports* (2019) **9**:11079.
746 doi:10.1038/s41598-019-47242-0.
747 18. Mohanta S, Yin C, Weber C, Hu D, Habenicht A, JR. Aorta Atherosclerosis Lesion Analysis in
748 Hyperlipidemic Mice. *Bio-protocol* (2016) **6**. doi:10.21769/bioprotoc.1833.
749 19. Gaul S, Leszczynska A, Alegre F, Kaufmann B, Johnson CD, Adams LA, et al. Hepatocyte pyroptosis
750 and release of inflammasome particles induce stellate cell activation and liver fibrosis. *Journal of*
751 *Hepatology*. doi:10.1016/j.jhep.2020.07.041.
752 20. Harman JL, Jørgensen HF. The role of smooth muscle cells in plaque stability: Therapeutic targeting
753 potential. *British journal of pharmacology* (2019) **176**:3741–53. doi:10.1111/bph.14779.
754 21. Doran AC, Meller N, McNamara CA. Role of smooth muscle cells in the initiation and early
755 progression of atherosclerosis. *Arteriosclerosis, thrombosis, and vascular biology* (2008) **28**:812–9.
756 doi:10.1161/ATVBAHA.107.159327.
757 22. SHEN XIA, BORNFELDT KE. Mouse Models for Studies of Cardiovascular Complications of Type 1
758 Diabetes. *Annals of the New York Academy of Sciences* (2007) **1103**:202–17.
759 doi:10.1196/annals.1394.004.
760 23. Oppi S, Lüscher TF, Stein S. Mouse Models for Atherosclerosis Research—Which Is My Line?
761 *Frontiers in Cardiovascular Medicine* (2019) **6**:46. doi:10.3389/fcvm.2019.00046.
762 24. Tse J, Martin-McNaulty B, Halks-Miller M, Kauser K, DelVecchio V, Vergona R, et al. Accelerated
763 atherosclerosis and premature calcified cartilaginous metaplasia in the aorta of diabetic male Apo E
764 knockout mice can be prevented by chronic treatment with 17β-estradiol. *Atherosclerosis* (1999)
765 **144**:303–13. doi:10.1016/S0021-9150(98)00325-6.
766 25. Vikramadithyan RK, Hu Y, Noh H-L, Liang C-P, Hallam K, Tall AR, et al. Human aldose reductase
767 expression accelerates diabetic atherosclerosis in transgenic mice. *The Journal of clinical*
768 *investigation* (2005) **115**:2434–43. doi:10.1172/JCI24819.
769 26. Lewis P, Stefanovic N, Pete J, Calkin AC, Giunti S, Thallas-Bonke V, et al. Lack of the Antioxidant
770 Enzyme Glutathione Peroxidase-1 Accelerates Atherosclerosis in Diabetic Apolipoprotein E–Deficient
771 Mice. *Circulation* (2007) **115**:2178–87. doi:10.1161/CIRCULATIONAHA.106.664250.
772 27. Vedantham S, Noh H, Ananthakrishnan R, Son N, Hallam K, Hu Y, et al. Human Aldose Reductase
773 Expression Accelerates Atherosclerosis in Diabetic Apolipoprotein E−/− Mice. *Arteriosclerosis,*
774 *thrombosis, and vascular biology* (2011) **31**:1805–13. doi:10.1161/ATVBAHA.111.226902.
775 28. Park L, Raman KG, Lee KJ, Lu Y, Ferran LJ, Chow WS, et al. Suppression of accelerated diabetic
776 atherosclerosis by the soluble receptor for advanced glycation endproducts. *Nature Medicine* (1998)
777 **4**:1025–31. doi:10.1038/2012.

778 29. Hammad SM, Hazen-Martin DJ, Sohn M, Eldridge L, Powell-Braxton L, Won W, et al. Nephropathy in
779 a Hypercholesterolemic Mouse Model with Streptozotocin-Induced Diabetes. *Kidney and Blood*
780 *Pressure Research* (2003) **26**:351–61. doi:10.1159/000073942.
781 30. Goldberg IJ, Hu Y, Noh H-L, Wei J, Huggins LA, Rackmill MG, et al. Decreased lipoprotein clearance is
782 responsible for increased cholesterol in LDL receptor knockout mice with streptozotocin-induced
783 diabetes. *Diabetes* (2008) **57**:1674–82. doi:10.2337/db08-0083.
784 31. Zhou C, Pridgen B, King N, Xu J, Breslow JL. Hyperglycemic Ins2AkitaLdlr−/− mice show severely
785 elevated lipid levels and increased atherosclerosis: a model of type 1 diabetic macrovascular
786 disease[S]. *Journal of lipid research* (2011) **52**:1483–93. doi:10.1194/jlr.M014092.
787 32. Engelbertsen D, To F, Dunér P, Kotova O, Söderberg I, Alm R, et al. Increased Inflammation in
788 Atherosclerotic Lesions of Diabetic *Akita-LDLr*$^{-/-}$ Mice Compared to Nondiabetic *LDLr*$^{-/-}$ Mice.
789 *Experimental Diabetes Research* (2012) **2012**:176162. doi:10.1155/2012/176162.
790 33. Bennett MR, Sinha S, Owens GK. Vascular Smooth Muscle Cells in Atherosclerosis. *Circulation*
791 *research* (2016) **118**:692–702. doi:10.1161/CIRCRESAHA.115.306361.
792 34. Dzau VJ, Braun-Dullaeus RC, Sedding DG. Vascular proliferation and atherosclerosis: new
793 perspectives and therapeutic strategies. *Nature Medicine* (2002) **8**:1249–56. doi:10.1038/nm1102-
794 1249.
795 35. Paigen B, Morrow A, Holmes PA, Mitchell D, Williams RA. Quantitative assessment of atherosclerotic
796 lesions in mice. *Atherosclerosis* (1987) **68**:231–40. doi:10.1016/0021-9150(87)90202-4.
797 36. Reddick RL, Zhang SH, Maeda N. Atherosclerosis in mice lacking apo E. Evaluation of lesional
798 development and progression. *Arteriosclerosis and thrombosis a journal of vascular biology* (1994)
799 **14**:141–7. doi:10.1161/01.atv.14.1.141.
800 37. Tangirala RK, Rubin EM, Palinski W. Quantitation of atherosclerosis in murine models: correlation
801 between lesions in the aortic origin and in the entire aorta, and differences in the extent of lesions
802 between sexes in LDL receptor-deficient and apolipoprotein E-deficient mice. *Journal of lipid*
803 *research* (1995) **36**:2320–8.
804 38. Getz GS, Reardon CA. Diet and Murine Atherosclerosis. *Arteriosclerosis, thrombosis, and vascular*
805 *biology* (2006) **26**:242–9. doi:10.1161/01.ATV.0000201071.49029.17.
806 39. Johansson F, Kramer F, Barnhart S, Kanter JE, Vaisar T, Merrill RD, et al. Type 1 diabetes promotes
807 disruption of advanced atherosclerotic lesions in LDL receptor-deficient mice. *Proceedings of the*
808 *National Academy of Sciences of the United States of America* (2008) **105**:2082–7.
809 doi:10.1073/pnas.0709958105.
810 40. BORNFELDT KE. Uncomplicating the Macrovascular Complications of Diabetes: The 2014 Edwin
811 Bierman Award Lecture. *Diabetes* (2015) **64**:2689–97. doi:10.2337/db14-1963.
812 41. Renard CB, Kramer F, Johansson F, Lamharzi N, Tannock LR, Herrath MG von, et al. Diabetes and
813 diabetes-associated lipid abnormalities have distinct effects on initiation and progression of
814 atherosclerotic lesions. *The Journal of clinical investigation* (2004) **114**:659–68.
815 doi:10.1172/JCI17867.
816 42. Apostolakis S, Spandidos D. Chemokines and atherosclerosis: focus on the CX3CL1/CX3CR1 pathway.
817 *Acta pharmacologica Sinica* (2013) **34**:1251–6. doi:10.1038/aps.2013.92.
818 43. Gerdes N, Sukhova GK, Libby P, Reynolds RS, Young JL, Schönbeck U. Expression of interleukin (IL)-18
819 and functional IL-18 receptor on human vascular endothelial cells, smooth muscle cells, and

macrophages: implications for atherogenesis. *The Journal of experimental medicine* (2002) **195**:245–57. doi:10.1084/jem.20011022.

44. Wang J, Sun C, Gerdes N, Liu C, Liao M, Liu J, et al. Interleukin 18 function in atherosclerosis is mediated by the interleukin 18 receptor and the Na-Cl co-transporter. *Nature Medicine* (2015) **21**:820–6. doi:10.1038/nm.3890.
45. Mallat Z, Corbaz A, Scoazec A, Besnard S, Lesèche G, Chvatchko Y, et al. Expression of interleukin-18 in human atherosclerotic plaques and relation to plaque instability. *Circulation* (2001) **104**:1598–603. doi:10.1161/hc3901.096721.
46. Ihara Y, Egashira K, Nakano K, Ohtani K, Kubo M, Koga J-i, et al. Upregulation of the ligand-RAGE pathway via the angiotensin II type I receptor is essential in the pathogenesis of diabetic atherosclerosis. *Journal of molecular and cellular cardiology* (2007) **43**:455–64. doi:10.1016/j.yjmcc.2007.07.044.
47. Bu D-x, Rai V, Shen X, Rosario R, Lu Y, D'Agati V, et al. Activation of the ROCK1 branch of the transforming growth factor-beta pathway contributes to RAGE-dependent acceleration of atherosclerosis in diabetic ApoE-null mice. *Circulation research* (2010) **106**:1040–51. doi:10.1161/CIRCRESAHA.109.201103.
48. Soro-Paavonen A, Watson AM, Li J, Paavonen K, Koitka A, Calkin AC, et al. Receptor for advanced glycation end products (RAGE) deficiency attenuates the development of atherosclerosis in diabetes. *Diabetes* (2008) **57**:2461–9. doi:10.2337/db07-1808.
49. Wang Z, Jiang Y, Liu N, Ren L, Zhu Y, An Y, et al. Advanced glycation end-product Nε-carboxymethyl-Lysine accelerates progression of atherosclerotic calcification in diabetes. *Atherosclerosis* (2012) **221**:387–96. doi:10.1016/j.atherosclerosis.2012.01.019.
50. Kumar S, Chen M, Li Y, Wong FH, Thiam CW, Hossain MZ, et al. Loss of ADAMTS4 reduces high fat diet-induced atherosclerosis and enhances plaque stability in ApoE−/− mice. *Scientific reports* (2016) **6**:31130. doi:10.1038/srep31130.
51. Dong H, Du T, Premaratne S, Zhao CX, Tian Q, Li Y, et al. Relationship between ADAMTS4 and carotid atherosclerotic plaque vulnerability in humans. *Journal of Vascular Surgery* (2018) **67**:1120–6. doi:10.1016/j.jvs.2017.08.075.
52. Ray BK, Shakya A, Turk JR, Apte SS, Ray A. Induction of the MMP-14 gene in macrophages of the atherosclerotic plaque: role of SAF-1 in the induction process. *Circulation research* (2004) **95**:1082–90. doi:10.1161/01.RES.0000150046.48115.80.
53. Canault M, Peiretti F, Poggi M, Mueller C, Kopp F, Bonardo B, et al. Progression of atherosclerosis in ApoE-deficient mice that express distinct molecular forms of TNF-alpha. *The Journal of pathology* (2008) **214**:574–83. doi:10.1002/path.2305.
54. Martins IJ, Hone E, Foster JK, Sünram-Lea SI, Gnjec A, Fuller SJ, et al. Apolipoprotein E, cholesterol metabolism, diabetes, and the convergence of risk factors for Alzheimer's disease and cardiovascular disease. *Molecular psychiatry* (2006) **11**:721–36. doi:10.1038/sj.mp.4001854.
55. Farmer BC, Johnson LA, Hanson AJ. Effects of apolipoprotein E on nutritional metabolism in dementia. *Current opinion in lipidology* (2019) **30**:10–5. doi:10.1097/MOL.0000000000000566.
56. Hui DY, Basford JE. Distinct signaling mechanisms for apoE inhibition of cell migration and proliferation. *Neurobiology of aging* (2005) **26**:317–23. doi:10.1016/j.neurobiolaging.2004.02.030.

861 57. Vozenilek AE, Blackburn CM, Schilke RM, Chandran S, Castore R, Klein RL, et al. AAV8-mediated
862 overexpression of mPCSK9 in liver differs between male and female mice. *Atherosclerosis* (2018)
863 **278**:66–72. doi:10.1016/j.atherosclerosis.2018.09.005.
864 58. Golforoush P, Yellon DM, Davidson SM. Mouse models of atherosclerosis and their suitability for the
865 study of myocardial infarction. *Basic research in cardiology* (2020) **115**:73. doi:10.1007/s00395-020-
866 00829-5.
867 59. Getz GS, Reardon CA. Do the Apoe-/- and Ldlr-/- Mice Yield the Same Insight on Atherogenesis?
868 *Arteriosclerosis, thrombosis, and vascular biology* (2016) **36**:1734–41.
869 doi:10.1161/ATVBAHA.116.306874.
870 60. Roche-Molina Marta, Sanz-Rosa David, Cruz Francisco M., García-Prieto Jaime, López Sergio, Abia
871 Rocío, et al. Induction of Sustained Hypercholesterolemia by Single Adeno-Associated Virus–
872 Mediated Gene Transfer of Mutant hPCSK9. *Arteriosclerosis, thrombosis, and vascular biology* (2015)
873 **35**:50–9. doi:10.1161/ATVBAHA.114.303617.
874 61. Rolandsson O, Haney MF, Hagg E, Biber B, Lernmark A. Streptozotocin induced diabetes in minipig: a
875 case report of a possible model for type 1 diabetes? *Autoimmunity* (2002) **35**:261–4.
876 doi:10.1080/0891693021000010703.
877 62. Saleem Mir M, Maqbool Darzi M, Khalil Baba O, Khan HM, Kamil SA, Sofi AH, et al. Streptozotocin
878 Induced Acute Clinical Effects in Rabbits (Oryctolagus cuniculus). *Iranian journal of pathology* (2015)
879 **10**:206–13.
880 63. Yuan F, Guo L, Park K-H, Woollard JR, Taek-Geun K, Jiang K, et al. Ossabaw Pigs With a PCSK9 Gain-
881 of-Function Mutation Develop Accelerated Coronary Atherosclerotic Lesions: A Novel Model for
882 Preclinical Studies. *Journal of the American Heart Association* (2018) **7**.
883 doi:10.1161/JAHA.117.006207.
884

885 # Figures

Figure 1

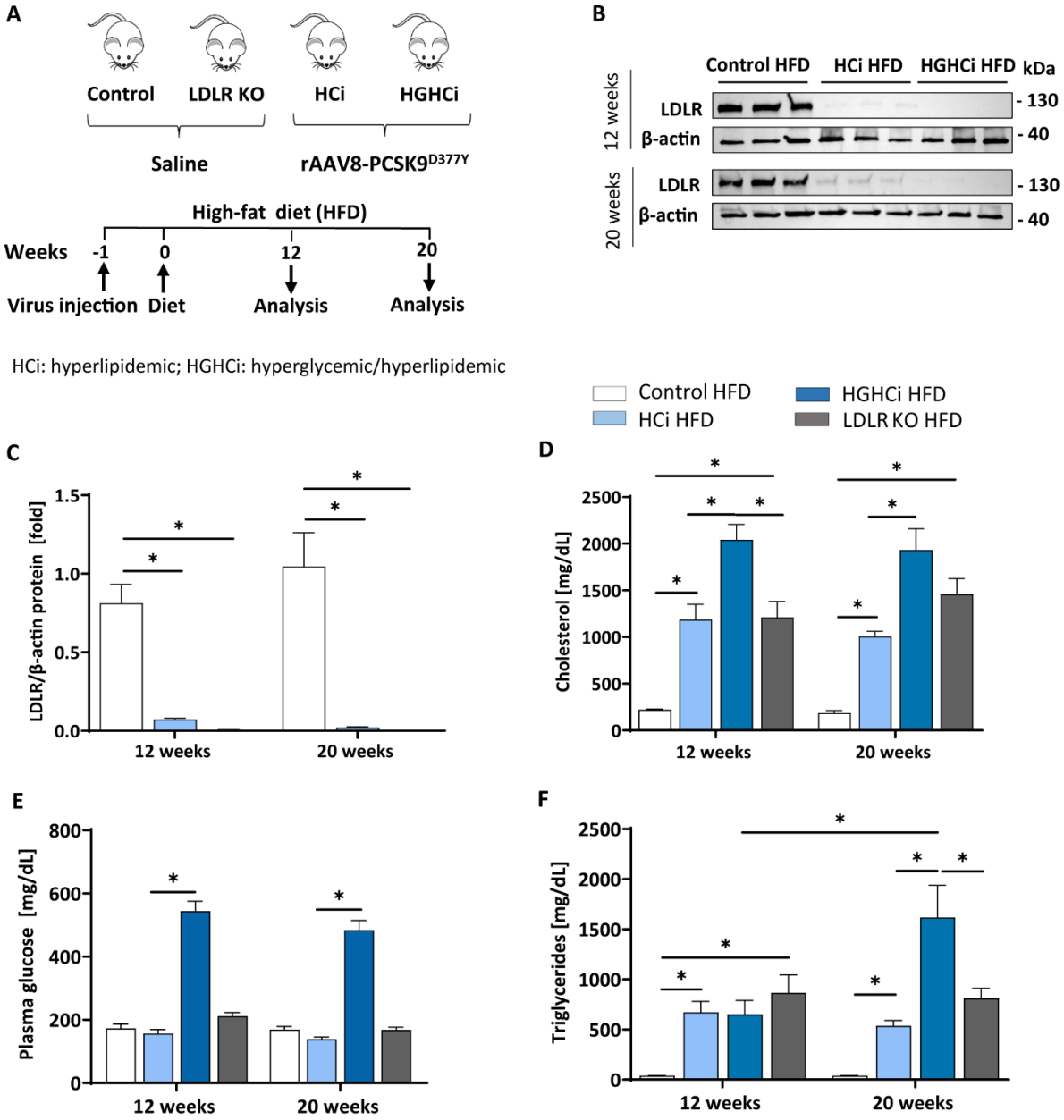

886
887

888 **Figure 1: Simultaneous treatment of rAAV8-PCSK9 virus and Streptozotocin induces a**
889 **hyperlipidemic and hyperglycemic mouse phenotype. A:** Schematic summary of the
890 experimental setup. Mice were analyzed after 12 or 20 weeks of interventions initiation. Wild type
891 mice without rAAV8-PCSK9^{D377Y} injection on high-fat diet (HFD, 21 % fat, 0.21 % cholesterol)
892 was used as control. Mice injected with rAAV8-PCSK9^{D377Y} and fed a HFD are termed HCi HFD
893 (hyperlipidemic), or injected with both rAAV8-PCSK9^{D377Y} and streptozotocin and fed a HFD are
894 termed HGHCi HFD (hyperlipidemic and hyperglycemic). LDLR KO mice on HFD served as

895 atherosclerosis reference control. **B:** Representative immunoblot of liver lysate showing hepatic
896 protein levels of low-density lipoprotein receptor (LDLR). β-actin was used as loading control. **C:**
897 Densitometric analysis of LDLR immunoblot was normalized on β-actin and referred to control
898 HFD group which is set at 1. Bar graphs are showing level of **D:** plasma cholesterol level [mg/dL],
899 **E:** blood glucose levels [mg/dL] and **F:** Triglycerides [mg/dL]. Data are presented as mean ± SEM
900 and two-way ANOVA was performed with Sidak's multiple comparison post-hoc test (*$p < 0.05$).
901 N= 6 for each group.

Figure 2

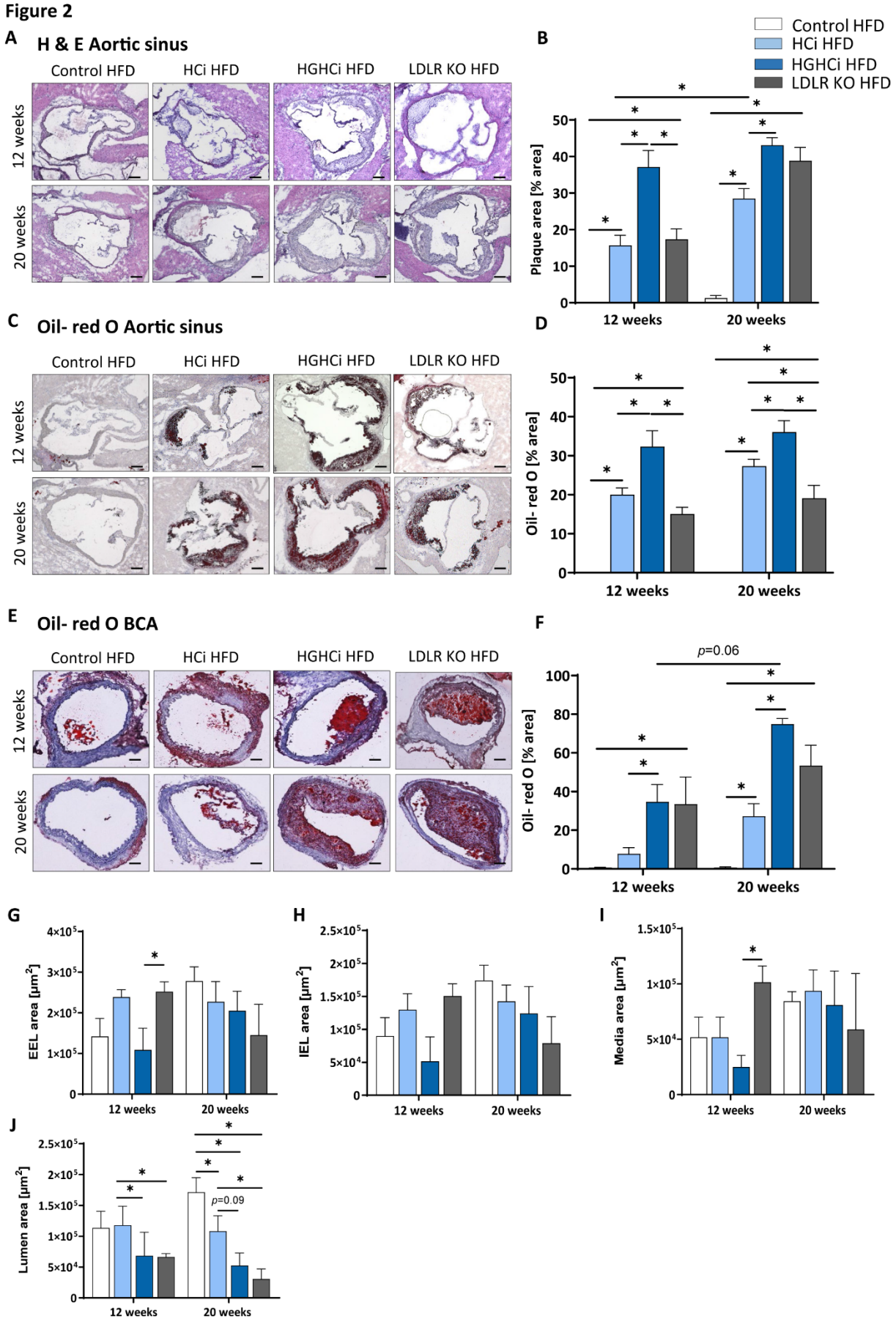
A
H & E Aortic sinus
Control HFD
HCi HFD
HGHCi HFD
LDLR KO HFD
12 weeks
20 weeks
B
Control HFD
HCi HFD
HGHCi HFD
LDLR KO HFD
Plaque area [% area]
12 weeks
20 weeks
C
Oil- red O Aortic sinus
D
Oil- red O [% area]
E
Oil- red O BCA
F
p=0.06
G
EEL area [µm²]
H
IEL area [µm²]
I
Media area [µm²]
J
Lumen area [µm²]
p=0.09

903 **Figure 2: Mice with combined hyperlipidemia and hyperglycemia show larger plaques than**
904 **hyperlipidemic mice. A-D**: Representative histological images showing cross-sections of aortic
905 sinus stained with Hematoxylin/ Eosin (H & E, **A**) and bar graphs summarizing data (**B**).
906 Representative histological images showing aortic sinus sections stained with Oil-red O (**C**) and
907 bar graphs summarizing data (**D**). **E-H:** Representative histological images showing truncus
908 brachiocephalic arteries (BCA) sections stained with Oil-red O (**E**) and bar graphs summarizing
909 data (**F**). Stainings were imaged at 4 × magnification (scale bar 100 µm) (**A, C, E**). HFD control
910 12 and 20 weeks (N= 7), HCi HFD 12 and 20 weeks (N= 5), and HGHCi HFD 12 and 20 weeks
911 (N= 6). Determination of the external elastic lamina (EEL) (**G**), internal elastic lamina (IEL) (**H**),
912 media area (**I**) and the lumen area (**J**) from Oil-red O stained cross-sections of the BCA (see
913 Supplementary Figure II). Data presented as mean ± SEM and two-way ANOVA were performed
914 with Sidak's multiple comparison post-hoc test (*$p < 0.05$).
915 Control HFD: Wild type mice without rAAV8-PCSK9^{D377Y} injection on high fat diet (HFD); HCi
916 HFD: rAAV8-PCSK9^{D377Y} injection plus HFD (hyperlipidemic); HGHCi HFD: rAAV8-
917 PCSK9^{D377Y} and streptozotocin injection and HFD (hyperlipidemic and hyperglycemic)

Figure 3

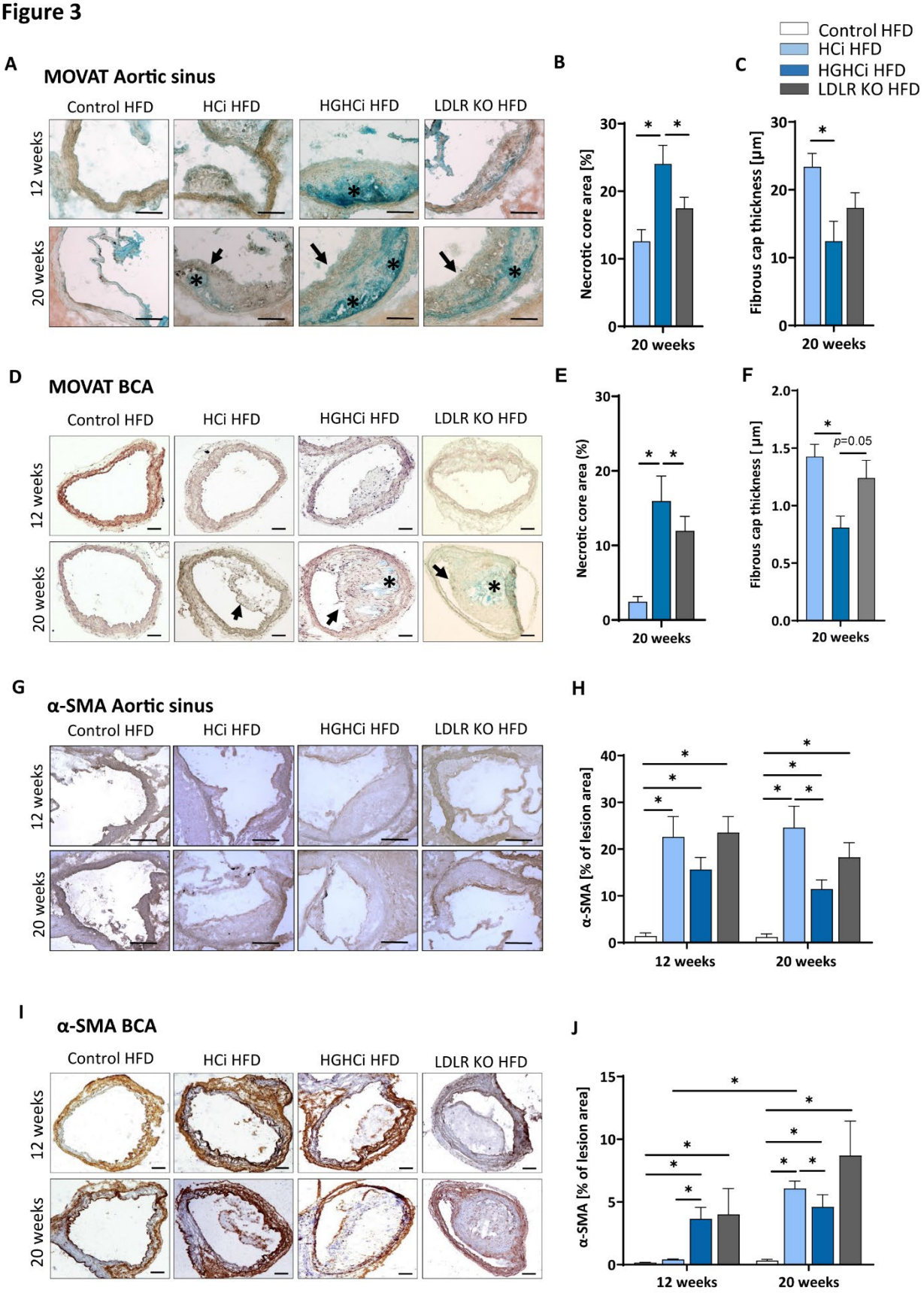
A
MOVAT Aortic sinus
Control HFD
HCi HFD
HGHCi HFD
LDLR KO HFD
12 weeks
20 weeks
B
Necrotic core area [%]
20 weeks
C
Fibrous cap thickness [µm]
20 weeks
D
MOVAT BCA
E
Necrotic core area (%)
F
Fibrous cap thickness [µm]
p=0.05
G
α-SMA Aortic sinus
H
α-SMA [% of lesion area]
12 weeks
20 weeks
I
α-SMA BCA
J

Figure 3: Increased necrotic core, reduced fibrous cap thickness, and α-SMA positive cells within plaques of hyperlipidemic and hyperglycemic mice as compared to hyperlipidemic mice.

A-C: Representative images showing MOVATs pentachrome staining of cross-sections of the aortic sinus (**A**, scale bar 100 µm, 10x magnification). Bar graphs summarizing morphometric analyses of MOVATs stained images for necrotic core area (indicated by *) (**B**) and fibrous cap thickness (indicated by a black arrow) (**C**). Necrotic core area is depicted as % of total lesion area. **D-F:** Representative images showing MOVATs pentachrome staining of cross-sections of truncus brachiocephalic arteries (BCA) (**D**, scale bar 200 µm, 4x magnification). Bar graphs summarizing morphometric analyses of MOVATs stained images for necrotic core area (indicated by *) (**E**) and fibrous cap thickness thickness (indicated by a black arrow) (**F**). Data presented as mean + SEM and one-way ANOVA was performed with Sidak's multiple comparison post-hoc test (*$p < 0.05$). **G,H:** Representative images showing immunohistochemical staining for α-SMA positive cells detected by HRP-DAB reaction (brown) on cross-sections of aortic sinus (**G**, **H**) (scale bar 100 µm, 10x magnification) and truncus brachiocephalic arteries (**I**, **J**) (scale bar 200 µm, 4x magnification). Corresponding bar graphs summarizing data (**H, J**). Data presented as mean + SEM and two-way ANOVA were performed with Sidak's multiple comparison post-hoc test (*$p < 0.05$). HFD control 12 and 20 weeks (N= 7), HCi HFD 12 and 20 weeks (N= 5), and HGHCi HFD 12 and 20 weeks (N= 6).

Control HFD: Wild type mice without rAAV8-PCSK9^{D377Y} injection on high fat diet (HFD); HCi HFD: rAAV8-PCSK9^{D377Y} injection plus HFD (hyperlipidemic); HGHCi HFD: rAAV8-PCSK9^{D377Y} and streptozotocin injection and HFD (hyperlipidemic and hyperglycemic).

Figure 4

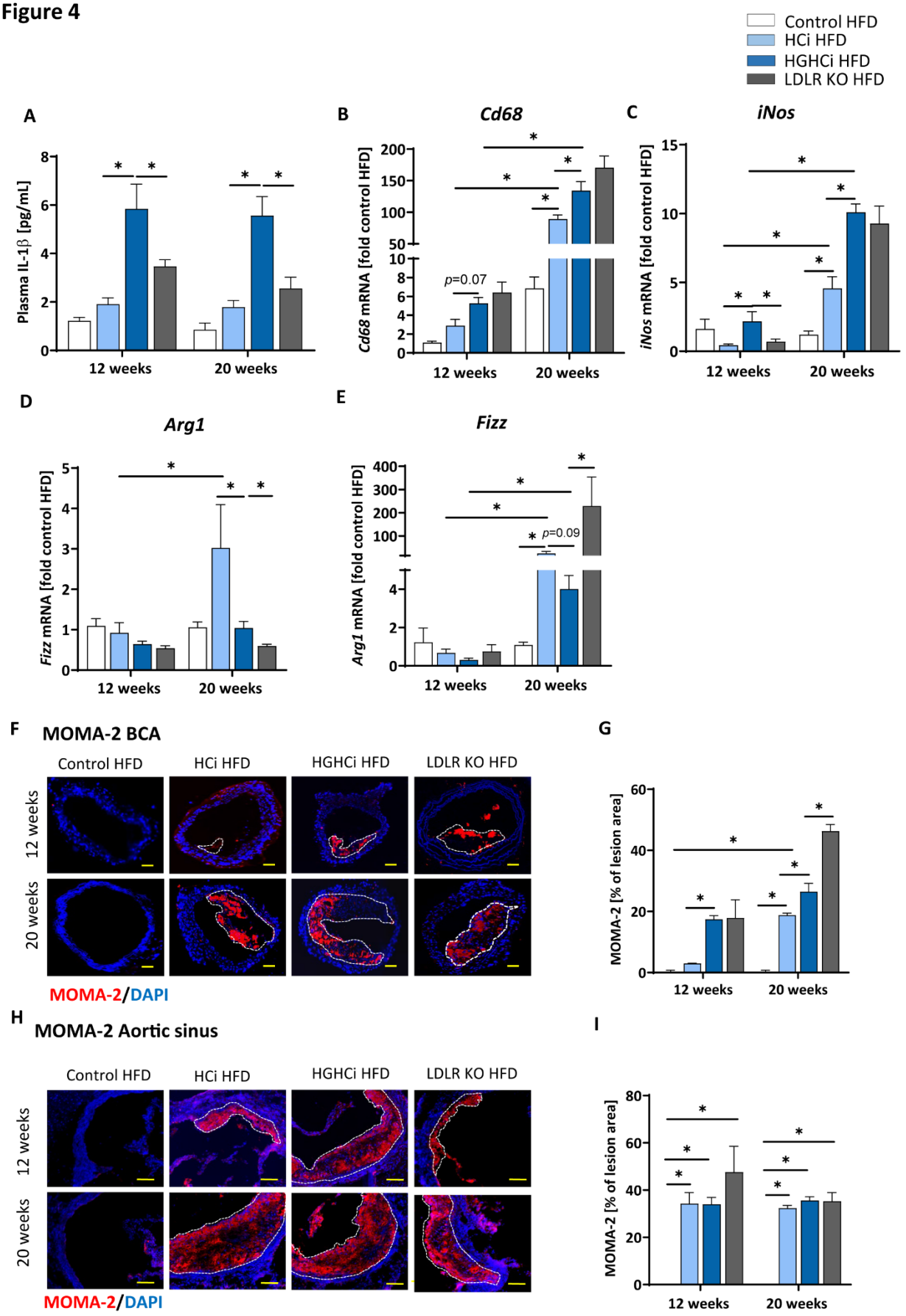
Control HFD
HCi HFD
HGHCi HFD
LDLR KO HFD
A
Plasma IL-1β [pg/mL]
12 weeks
20 weeks
B
Cd68
Cd68 mRNA [fold control HFD]
p=0.07
C
iNos
iNos mRNA [fold control HFD]
D
Arg1
Fizz mRNA [fold control HFD]
E
Fizz
Arg1 mRNA [fold control HFD]
p=0.09
F
MOMA-2 BCA
Control HFD
HCi HFD
HGHCi HFD
LDLR KO HFD
12 weeks
20 weeks
MOMA-2/DAPI
G
MOMA-2 [% of lesion area]
H
MOMA-2 Aortic sinus
I

941

942 **Figure 4: Increased IL-1β plasma level and expression of pro-inflammatory markers in**
943 **hyperlipidemic and hyperglycemic mice as compared to hyperlipidemic mice.**

944 **A:** Plasma IL-1β [pg/mL] level at 12 and 20 weeks. **B-E**: mRNA expression of macrophage
945 polarization markers. M1 macrophage polarization is depicted by *CD68* (**B**) and *iNos* (**C**) mRNA
946 expression. *Arg1* (**D**) and *Fizz* (**E**) mRNA expression levels are shown as M2 polarization marker.
947 The data are presented as mean ± SEM and were normalized on the mean of two housekeeping
948 genes (*Hprt* and *B2m*). HFD control served as reference and was set at 1. **F, G:** Representative
949 images showing immunofluorescence staining of truncus brachiocephalic arteries (BCA) sections
950 for macrophage marker MOMA-2 (**F,** MOMA-2= red; DAPI nuclear counterstain= blue; plaque
951 region is circled with a white dashed line, scale bar 200 µm, 4 × magnification) and bar graphs
952 summarizing data (**G**). Representative images showing immunofluorescence staining of cross-
953 sections of aortic sinus for MOMA-2 (**H,** MOMA-2= red; DAPI nuclear counterstain= blue; plaque
954 region is circled with a white dashed line, scale bar 100 µm, 10 × magnification) and bar graphs
955 summarizing data (**I**). Data presented as mean ± SEM and two-way ANOVA were performed with
956 Sidak's multiple comparison post-hoc test (*$p < 0.05$). HFD control 12 and 20 weeks (N= 7), HCi
957 HFD 12 and 20 weeks (N= 5), and HGHCi HFD 12 and 20 weeks (N= 6).

958 Control HFD: Wild type mice without rAAV8-PCSK9^{D377Y} injection on high fat diet (HFD); HCi HFD:
959 rAAV8-PCSK9^{D377Y} injection plus HFD (hyperlipidemic); HGHCi HFD: rAAV8-PCSK9^{D377Y} and
960 streptozotocin injection and HFD (hyperlipidemic and hyperglycemic).

Figure 5

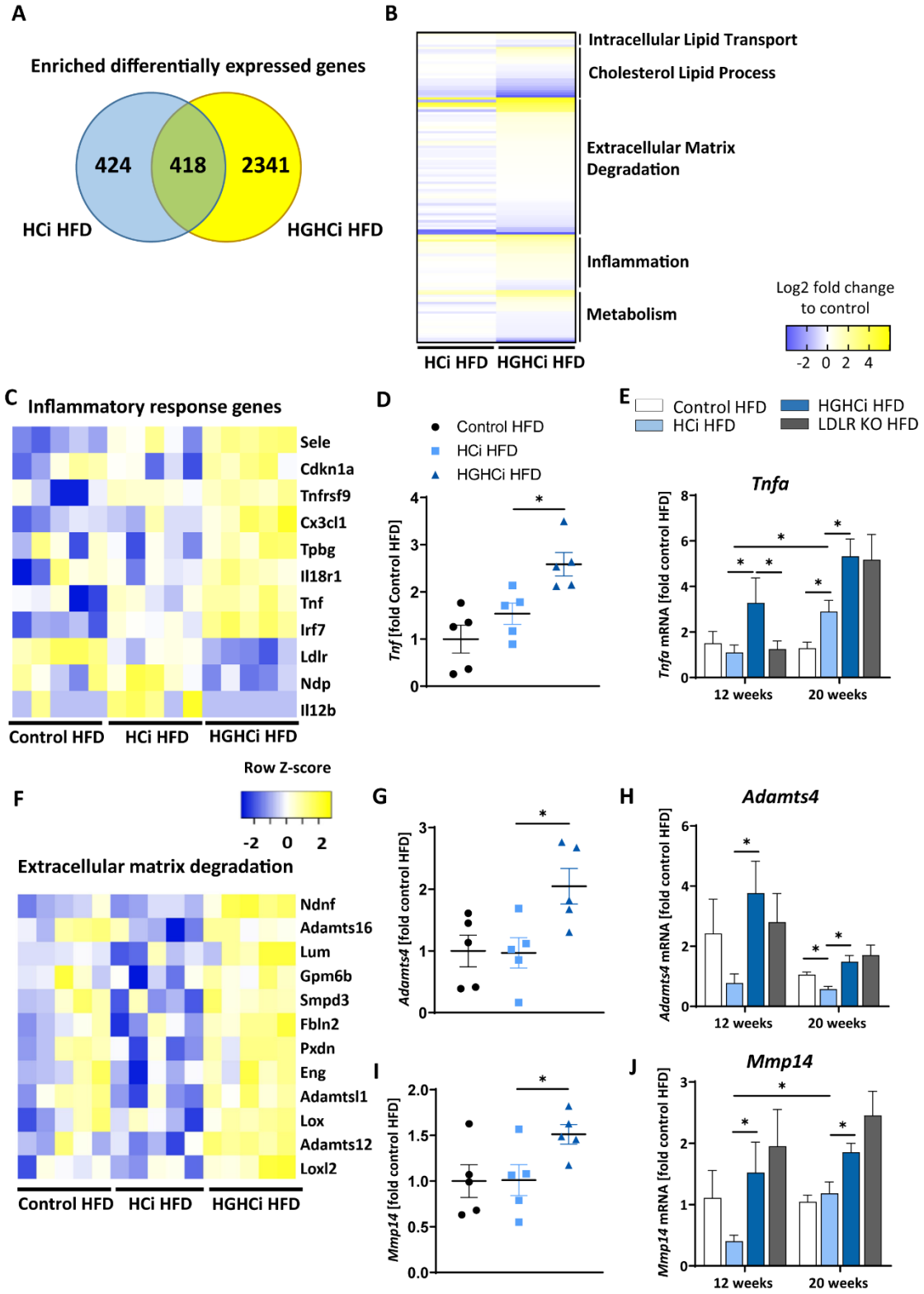

Figure 5: Combined hyperglycemia and hyperlipidemia induce large set of differentially expressed genes and activates inflammatory response and extracellular matrix degradation

964 **pathways.** RNA sequencing in aortic tissue of control HFD, HCi HFD and HGHCi HFD mice after
965 12 weeks. Wild type mice without AAV8-PCSK9^{D377Y} injection on high fat diet (control HFD) or
966 injected with rAAV8-PCSK9^{D377Y} and on HFD (hyperlipidemic, HCi HFD) or injected with both
967 rAAV8-PCSK9^{D377Y} and streptozotocin and fed HFD (hyperlipidemic and hyperglycemic, HGHCi
968 HFD). **A**: Venn diagram showing overlap of genes significantly changed in HGHCi HFD or HCi
969 HFD mice in relation to gene expression in control HFD mice. **B:** Heat map summarizing
970 differentially expressed gene (DEGs) identified by RNA sequencing and DEGs related biological
971 processes using Gene Ontology and EnrichR analysis. **C**: Heat map showing list of DEGs related
972 to inflammatory response (GO:0006954) using Gene Ontology and EnrichR analysis. **D:** *Tnf*
973 expression level (FPKM normalized on Control HFD) from RNASeq at 12 weeks (N=5/ group)
974 and its (**E)** qPCR validation in all groups at both time points (12 and 20 weeks). **F**: Heat map
975 showing list of DEGs related to extracellular matrix degradation pathways (GO:0030198) using
976 Gene Ontology and EnrichR analysis. RNA expression levels of selected ECM degradation genes
977 *Adamts4* (**G, H**) and *Mmp14* (**I, J**) (FPKM normalized on Control HFD) from RNASeq at 12 weeks
978 (N=5/ group) (**G, I**) and its qPCR validation (**H, J**) in all groups at both time points (12 and 20
979 weeks). Gene count values larger than the average control are represented in yellow, while lower
980 counts than the average control are represented in blue. Whenever transcript values are close to the
981 control value, samples are colored in white. The data are presented as mean ± SEM and qPCR data
982 were normalized on the mean of two housekeeping genes (*Hprt* and *B2m*). HFD control served as
983 reference control. Two-way ANOVA was performed with Sidak's multiple comparison post-hoc
984 test (*$p < 0.05$).

Figure 6

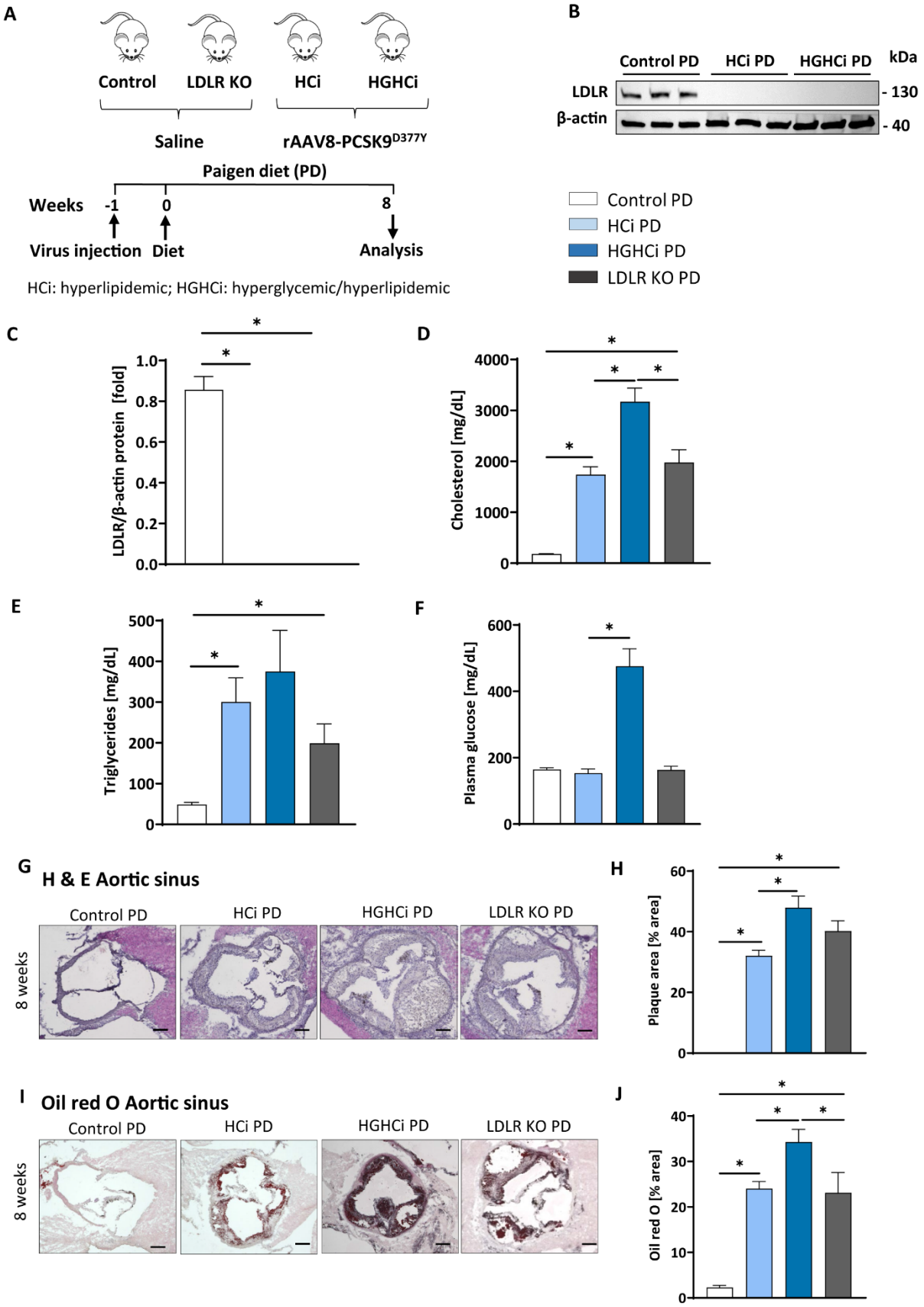
A
Control
LDLR KO
HCi
HGHCi
Saline
rAAV8-PCSK9D377Y
Paigen diet (PD)
Weeks -1 0 8
Virus injection
Diet
Analysis
HCi: hyperlipidemic; HGHCi: hyperglycemic/hyperlipidemic
B
Control PD
HCi PD
HGHCi PD
kDa
LDLR
β-actin
- 130
- 40
Control PD
HCi PD
HGHCi PD
LDLR KO PD
C
LDLR/β-actin protein [fold]
D
Cholesterol [mg/dL]
E
Triglycerides [mg/dL]
F
Plasma glucose [mg/dL]
G
H & E Aortic sinus
Control PD
HCi PD
HGHCi PD
LDLR KO PD
8 weeks
H
Plaque area [% area]
I
Oil red O Aortic sinus
Control PD
HCi PD
HGHCi PD
LDLR KO PD
8 weeks
J
Oil red O [% area]

986 **Figure 6: Paigen diet accelerates plaque formation after 8 weeks in the rAAV8-PCSK9**
987 **streptozotocin induced hyperglycemic atherosclerosis mouse model. A**: Schematic summary of
988 the experimental setup. Mice were analyzed after 8 weeks of interventions initiation. **B**:
989 Representative immunoblot showing hepatic protein levels of low-density lipoprotein receptor
990 (LDLR). β-actin was used as loading control and bar graphs summarizing data. Data were
991 normalized on β-actin and control PD mice were set at 1 (**C**). Bar graphs summarizing data of
992 plasma cholesterol level [mg/dL, **D**], triglycerides [mg/dL, **E**), and blood glucose levels [mg/dL,
993 **F**]. **G-J:** Representative histological images showing aortic sinus sections stained with
994 Hematoxylin Eosin (H & E, **G**) and bar graphs summarizing data (**H**). Representative histological
995 images showing aortic sinus sections stained with Oil-red-O (**I**) and bar graphs summarizing data
996 (**J**). Data presented as mean ± SEM and one-way ANOVA was performed with Sidak's multiple
997 comparison post-hoc test (*$p < 0.05$). Scale bar 200 µm. Control paigen diet (PD) (N=6), HCi PD
998 (N=6), HGHCi PD (N=6), LDLR KO PD (N=5). Control PD: Wild type mice without rAAV8-
999 PCSK9^{D377Y} injection on PD; HCi PD: mice injected with rAAV8-PCSK9^{D377Y} and fed PD
1000 (hyperlipidemic); HGHCi PD: mice injected with both rAAV8-PCSK9^{D377Y} and streptozotocin and
1001 fed PD (hyperlipidemic and hyperglycemic); LDLR KO PD: LDLR KO mice fed PD.
1002

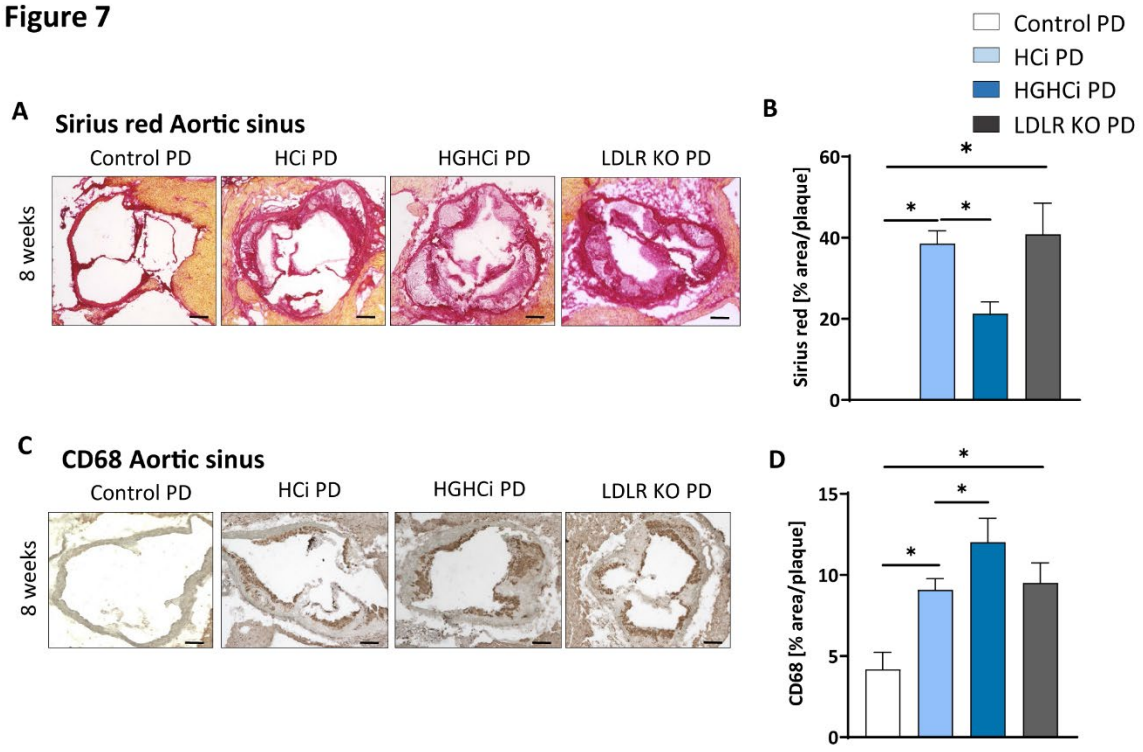

1003

1004 **Figure 7: Hyperlipidemic and hyperglycemic mice fed a Paigen diet (PD) show less collagen**
1005 **and increased inflammation within aortic plaques compared to hyperlipidemic mice.**
1006 **A**: Representative images showing picrosirius red staining for collagen in aortic sinus sections and
1007 bar graphs summarizing data (**B**). Scale bar 200 µm. **C:** Representative images showing

1008 immunohistochemical staining of aortic sinus sections for macrophages marker CD68 (positive
1009 cells detected by HRP-DAB reaction, brown) and bar graphs summarising data (**D**). Data presented
1010 as mean ± SEM and one-way ANOVA was performed with Sidak's multiple comparison post-hoc
1011 test (*$p < 0.05$). Scale bar 100 µm. Control paigen diet (PD) (N= 7), HCi PD (N= 4), HGHCi PD
1012 (N=4), LDLR KO PD (N=5). Control PD: Wild type mice without rAAV8-PCSK9^{D377Y} injection
1013 on PD; HCi PD: mice injected with rAAV8-PCSK9^{D377Y} and fed PD (hyperlipidemic); HGHCi PD:
1014 mice injected with both rAAV8-PCSK9^{D377Y} and streptozotocin and fed PD (hyperlipidemic and
1015 hyperglycemic); LDLR KO PD: LDLR KO mice fed PD.

1016

Supplementary Material

Content:

Supplementary Table 1. Characteristics of mice cohort.

Supplementary Figure I. PD fed HGHCi mice showed higher mortality than HFD fed mice.

Supplementary Figure II. Determination of the external and internal elastic lamina, lumen area and media area.

Supplementary Figure III. Comparison of aortic plaque score and total vessel lumen area.

Supplementary Figure IV. Intraplaque hemorrhage is not increased in HGHCi HFD mice.

Supplementary Figure V. Hyperglycemia alone does not affect plasma cholesterol levels in mice fed a Paigen diet.

Major resources table

Supplementary Table 1. Characteristics of mice cohort.

High-fat diet	Body weight [g]	Liver weight [g]	Liver/body weight ratio
12 weeks			
Normal chow	31.8 ± 3.7[a]	1.5 ± 0.4[a]	0.04
Saline HFD	40.4 ± 2.3	2.8 ± 0.5	0.06
HCi HFD	39.1 ± 3.3	2.6 ± 0.5	0.07
HGHCi HFD	24.7 ± 0.9[b]	2.8 ± 0.2	0.11
LDLR KO HFD	36.3 ± 5.5	2.1 ± 0.6	0.05
20 weeks			
Normal chow	32.5 ± 2.8[a]	1.7 ± 0.1[a]	0.05
Saline HFD	42.6 ± 4.8	3.0 ± 1.1[b]	0.07
HCi HFD	45.3 ± 3.9[c]	4.1 ± 0.7[ac]	0.09
HGHCi HFD	27.3 ± 3.5[b]	2.7 ± 0.2[b]	0.10
LDLR KO HFD	39.2 ± 3.4	3.2 ± 0.7[c]	0.08

Paigen diet	Body weight [g]	Liver weight [g]	Liver/body weight ratio
8 weeks			
Saline PD	31.1 ± 1.2	2.0 ± 0.1	0.06
HCi Paigen	32.0 ± 3.5	1.7 ± 0.2	0.05
HGHCi Paigen	19.7 ± 3.1[b]	2.7 ± 0.1[b]	0.14
LDLR KO Paigen	27.9 ± 1.6[b]	1.6 ± 0.2	0.06

Supplementary Table 1. Data are shown as mean ± SEM and statistical comparisons between the groups were calculated using the one-way ANOVA and Sidak's posthoc test. [a] $p<0.05$ vs Saline HFD/PD, [b] $p<0.05$ vs HCi HFD/PD, [c] $p<0.05$ vs 12 weeks. HFD: high-fat diet; HCi: hyperlipidemia model; HGHCi: hyperglycemia + hyperlipidemia model; PD: Paigen diet

Supplementary Figure I. PD fed HGHCi mice showed higher mortality than HFD fed mice.

A

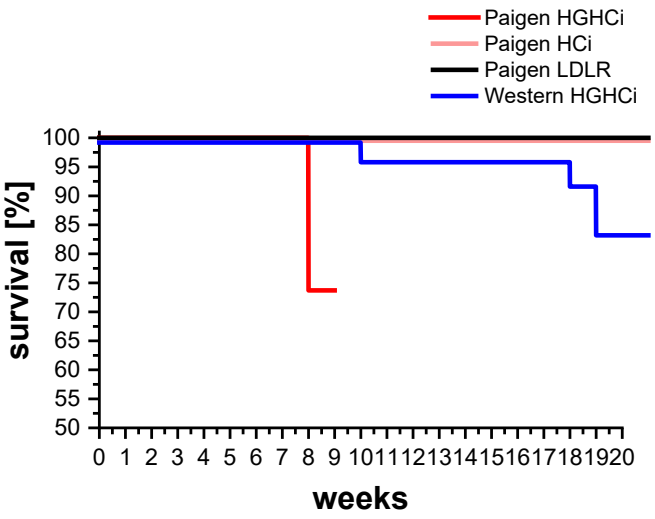

Supplementary Figure I. A: Kaplan-Meier survival curves of HGHCi, HCi and LDL receptor KO mice on Paigen diet compared to HGHCi mice on Western diet (high-fat diet, HFD).

Supplementary Figure II. Determination of the external and internal elastic lamina, lumen area and media area.

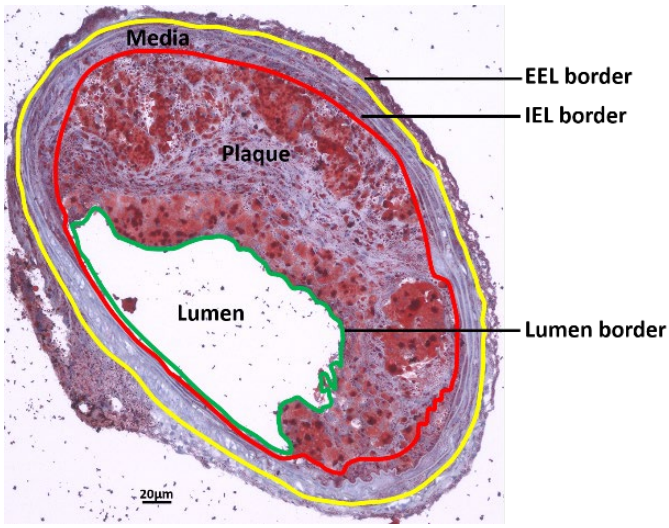

Supplementary Figure II. Representative image showing Oil-Red O stained BCA (**G**) for the measurement of the external elastic lamina (EEL, yellow line), internal elastic lamina (IEL, red line) and the lumen area (circled by a green line).

Supplementary Figure III. Comparison of aortic plaque score and total vessel lumen area.

A

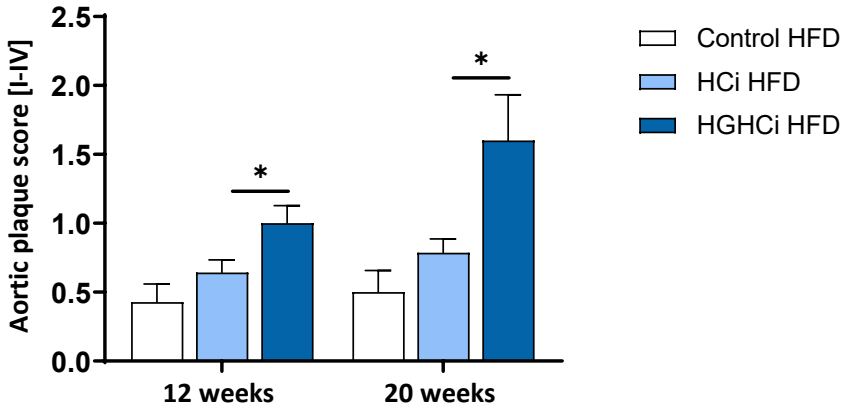

B

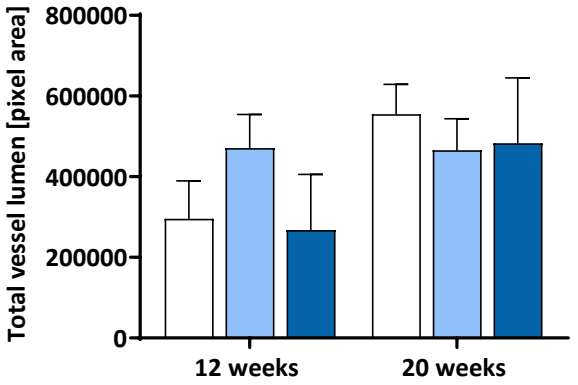

Supplementary Figure III. A: Aortic plaque score and total vessel lumen area [Pixel] of the truncus brachiocephalicus of HGHC and HCi mice on Western diet (high-fat diet, HFD) after 12 and 20 weeks. Aortic plaque score was determined as described below. 0= no lesions; 1= Lesions only in bifurcation; 2= like 1 + at least one long-stretch lesion; 3= like 1 + at least two long-stretch lesions; 4= like 1 + three to four long-stretch lesions

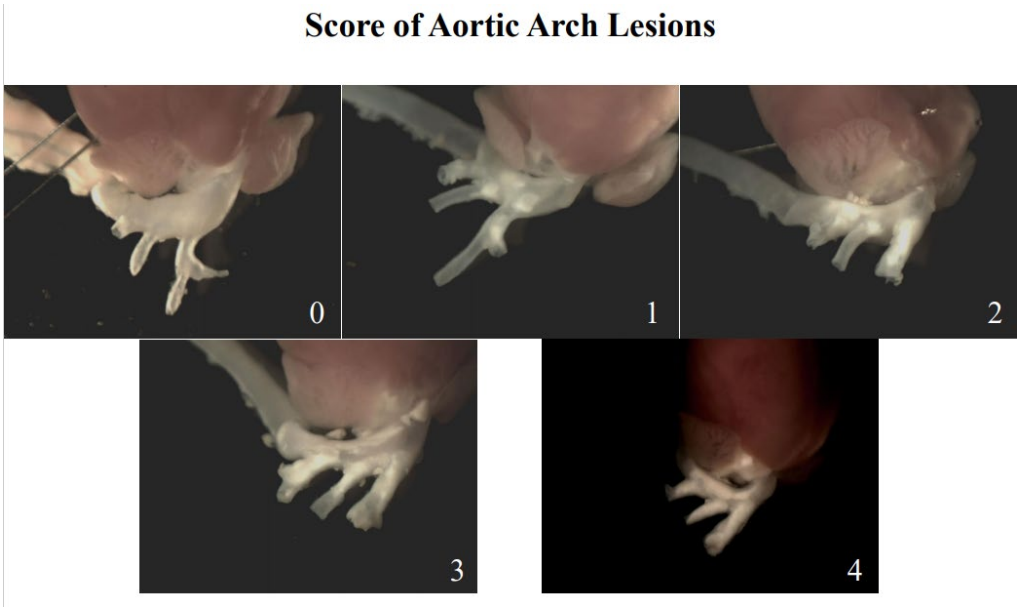

Supplementary Figure IV. Intraplaque hemorrhage is not increased in HGHCi HFD mice.

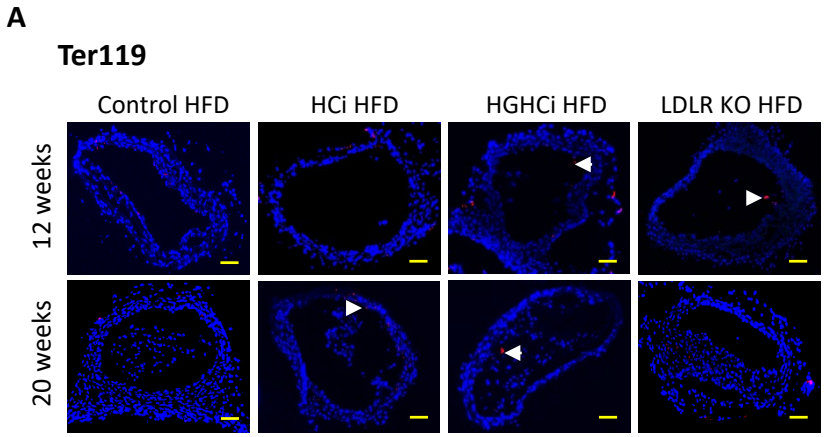

Supplementary Figure IV. A: Representative images showing immunofluorescence staining of truncus brachiocephalic arteries sections for hemorrhage marker Terr-119 (**A,** Terr-119= red; DAPI nuclear counterstain= blue, white arrows). Scale bar 200 µm. Control 12 and 20 weeks (N= 7), HCi 12 weeks (N= 5) and 20 weeks (N= 6), HGHCi 12 weeks (N= 7) and 20 weeks (N= 6).
Control HFD: Wild type mice without rAAV8-PCSK9^{D377Y} injection on high fat diet (HFD); HCi HFD: rAAV8-PCSK9^{D377Y} injection plus HFD (hyperlipidemic); HGHCi HFD: rAAV8-PCSK9^{D377Y} and streptozotocin injection and HFD (hyperlipidemic and hyperglycemic).

Supplementary Figure V. Hyperglycemia alone does not affect plasma cholesterol levels in mice fed a Paigen diet.

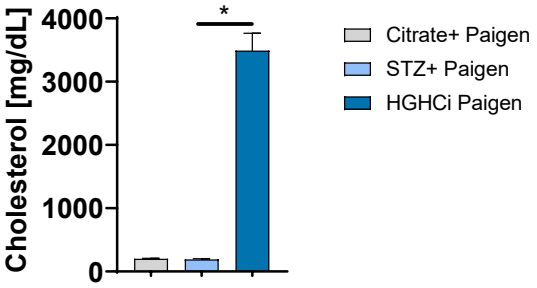

Supplementary Figure V. Hyperglycemia alone does not affect plasma cholesterol levels in mice fed a Paigen diet. Comparison of cholersterol levels in HGHCi mice (N=13), streptozotocin (STZ) treated mice (N=5) and citrate controls (N=3) fed with Paigen diet. Plasma cholesterol leves [mg/dL] were analyzed 12 weeks after induction of hypergylcemia with STZ.